

**GRAVIMETRIC INVESTIGATION OF GEOLOGICAL  
STRUCTURES WITHIN MAGADI TROUGH IN THE  
SOUTHERN KENYA RIFT**

**By:**

**OMOLLO PHILIP OMONDI**

**I56/64490/2010**

**A Dissertation Submitted in Partial Fulfilment for a degree in Masters of  
Science Geology**

**(APPLIED GEOPHYSICS)**

**UNIVERSITY OF NAIROBI**

**AUGUST 2012**

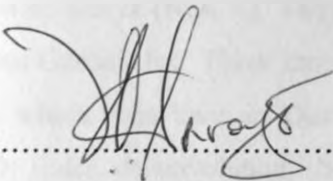
**DECLARATION**

The content of this dissertation is my original work and by any means has not been submitted to any other university for award of degree.

Signature.....  ..... Date: 08 / 08 / 2012 .....

**OMOLLO PHILIP OMONDI**

I ascertain that the candidate under my supervision has submitted his dissertation for examination with my knowledge as university supervisor

Signature.....  ..... Date: 8 / 8 / 2012 .....

**PROF. JUSTUS O. BARONGO**

**Department of Geology, University of Nairobi**

## ABSTRACT

Gravity method has been used for many years in the field of exploration like in oil exploration, geothermal exploration and in mineral exploration. It is one of the cheapest methods for data acquisition compared to other methods. In this study, gravity method was applied in mapping the study area with the aim of delineating sub surface geological structures, which are associated with hydrocarbon traps, their depth and location within the study area.

Magadi trough is situated in the southern part of the Kenyan tertiary rift about 110 km south of Nairobi, where it neighbours Tanzania to the south. It is occupied by broad half-graben depression highly filled with sediments and tilted blocks of late Miocene to early Pliocene.

The complete Bouguer anomaly in mGal was obtained as secondary data from National Oil Corporation of Kenya (NOCK). The data was gridded and maps were obtained using Oasis Montaj from Geosoft Inc. These maps were used to interpret the subsurface anomalies. The techniques which were used in Oasis Montaj to develop various maps are the analytical signal, 3D Euler deconvolution, horizontal derivative, vertical derivative and upward continuation.

From the interpretations, depocenters were mapped to the northern and southern part of Complete Bouguer Anomaly Map figure 5.1. Determination of depth to basement of the study area was done by use of 3D Euler deconvolution. The major structures mapped were faults and dyke. The fault is trending in NE-SW direction. The highest recorded value of depth to basement of the study area was about 8.1 km. The techniques applied revealed that the area accommodates depocenters along a fault to the north, to the south and at the central part, with an anticline to the west of the study area and a dyke to the south east. These revealed that area is structurally controlled and was affected tectonically. The fault was evident in the long stretch of the gravity low region which trends in the NE-SW. The sediment thickness in the study area was found to range from about 2km to 7 km. The presence of these structures shows that the area has a great potential of hydrocarbon traps.

## **DEDICATION**

It is with humbleness and honour that I dedicate this project to the Almighty Heavenly God for His mercy, grace, love, wisdom and giving me strength to complete this study. To my late grandfather and true friend Daudi Oyare Nyakinda who inspired me from childhood. This work is also dedicated to my Wife and daughter, Parents, grandmother Caren Nyodero, relatives and family members.

## ACKNOWLEDGEMENT

My thanks and appreciation is to all teaching staff of Geology Department, University of Nairobi, for their support and assistance during my studies.

I am grateful to my supervisor: Professor Justus Ombiko Barongo for his guidance and assistance during my study.

My acknowledgement is also to Dr. Nyamai the Chairman of Geology Department, and Dr. Kuria for their encouragement.

I sincerely appreciation the invaluable support from the National Oil Corporation of Kenya (NOCK) by way of providing the data I needed. In this regard, I particularly wish to thank Mr. Edmond Makhanu.

I want to recognize and appreciate the assistance of my Msc. colleagues whom I studied with: Dhieu Ater, Charity Cheruiyot, Junior Kimata, Josky Kisali and Gregory Odawo for their encouragement.

Others who deserve special acknowledgement are my dear wife, Susan Okoiti, and my daughter, Saphine Wande, for being understanding and supportive during the entire period of my studies.

Thanks also to my parents Ben Oyare and Mama Penina for their good upbringing and unceasing prayers.

I would also acknowledge assistance I got from my lecturers, friends especially Engineer Julian Masimba for being with me at point of need, my siblings and whoever helped me in any way and has not been mentioned.

To all, may our saviour Jesus Christ bless you with his unwavering mercy and truth.

## TABLE OF CONTENTS

DECLARATION.....	ii
ABSTRACT.....	iii
DEDICATION.....	iv
ACKNOWLEDGEMENT.....	v
LIST OF FIGURES.....	viii
LIST OF TABLE.....	viii
CHAPTER ONE.....	1
1.1 INTRODUCTION.....	1
1.2 Problem Statement.....	1
1.3 Location.....	2
1.4 Climate.....	4
1.5 Vegetation.....	4
1.6 Drainage.....	4
1.7 Land Use and Land Resources.....	5
1.8 Physiography.....	5
1.9 Soil.....	8
1.10 Literature Review.....	8
1.11 Justification and Significance.....	11
1.12 Aims and Objectives.....	12
1.12.1 Aim.....	12
1.12.2 Specific Objective.....	12
CHAPTER TWO.....	13
2.0 GEOLOGY OF MAGADI.....	13
2.1 Regional Geology.....	13
2.2 Geology of the Study Area.....	15
2.3 Structural Geology.....	18
CHAPTER THREE.....	20
3.0 GRAVITY METHODS.....	20
3.1 Background.....	20
3.2 Basic Theory.....	21
3.2.1 Newton's Law.....	21
3.2.2 Three Dimensional Euler deconvolution.....	26
3.2.3 Analytical signal.....	29
3.2.4 Horizontal gradient of gravity.....	30
3.2.5 Upward continuation.....	30
3.2.6 Vertical derivative.....	31
3.3 Interpretation methods.....	31
3.3.1 Qualitative Interpretation.....	31
3.3.2 Quantitative Interpretation.....	32
3.3.3 Direct and Indirect Methods.....	33
CHAPTER FOUR.....	34
4.0 DATA ACQUISITION AND PROCESSING.....	34
4.1 Data Acquisition.....	34
4.1.0 Introduction.....	34
4.1.1 Data source.....	34
4.2 Preliminary Data Acquisition.....	35
4.2.1 Gravity Instrument.....	35
4.3 Data Processing.....	37
4.3.1 Introduction.....	37

4.3.2	Data Correction .....	37
4.3.3	Gravity Anomaly .....	40
	CHAPTER FIVE .....	43
5.0.	DATA INTERPRETATION, RESULTS AND DISCUSSION .....	43
5.1.	Introduction .....	43
	CHAPTER SIX .....	52
6.0.	DISCUSSIONS, CONCLUSIONS AND RECOMMENDATIONS .....	52
6.1.	DISCUSSIONS .....	52
6.2.	CONCLUSION .....	55
6.3.	RECOMMENDATION .....	56
	REFERENCES .....	57
	APPENDIX .....	64
A.	Sedimentary Map of Kenya Showing the Study Area .....	64
B.	Gravity Data of Magadi Basin Covering the Study Area (NOCK, 1974) .....	65

## LIST OF FIGURES

Figure 1.1: Location Map of study area (from Githinji et al., 2011).....	3
Figure 1.2: Physiographical map of Magadi Basin .....	7
Figure 2.1: Geological Map of Southern Part of Kenya Rift Valley (modified from Baker and Mitchell, 1976).....	17
Figure 4.1: LaCoste and Romberg gravimeter.....	36
Figure 4.2: Schematic diagram illustrating the methodology .....	42
Figure 5.1: Complete Bouguer Anomaly Map.....	44
Figure 5.2: Upward Continuation map Continued at 1 km using a grid cells size of 5.....	45
Figure 5.3 : Horizontal Derivative Map of first order of grid cell size 5.....	47
Figure 5.4: Analytical Signal Map. A grid cell size of 5 was used in obtaining the analytical signal map. ....	48
Figure 5.5: Vertical Derivative Map .....	49
Figure 5.6: 3D Euler Deconvolution Depth Map at a grid cell size of 5.....	50

## LIST OF TABLE

Table 2-1: Geology of Magadi (modified from Baker, 1963) .....	15
--	----



## CHAPTER ONE

### 1.1 INTRODUCTION

Sedimentary basins in rift systems are now major targets of hydrocarbon exploration because most hydrocarbon occurrences are associated with sediments. Magadi trough in the southern part of the Kenyan rift is a sedimentary basin in which less interest has been shown for hydrocarbon exploration. The study area is in the semi arid environment bounded to the west by Nguruman escarpment, to the east by Lake Magadi and to the south, where it borders with Tanzania, are Shompole and Lenderut volcanoes. Lake Magadi is the lowest part of the region in altitude and most rivers drain into it. The community in the area is largely dependent on animals due to their nomadic way of life. With consideration of the location of Magadi trough, and other works in the area geared towards geothermal prospecting by Omenda (2007), and structural mapping and seismotectonic studies by Kuria (2011), it was important for the area to be investigated by use of gravity prospecting method for reconnaissance purposes prior to detailed seismic investigation to delineate sub-surface structures.

### 1.2 Problem Statement

Kenya Tertiary rift has shown good potential of hydrocarbon occurrence which is supported by the presence of oil in Turkana basin, gas discoveries in Tanzania, and significant proven oil reserves along the border of Uganda and Congo, in the western complex of the Great rift system. This has encouraged interest in the East African nations for hydrocarbon exploration. In Magadi area, there is need to investigate geological structures to determine their subsurface geometry, faulting intensity and constituents (fluids sediments) for proper characteristics of the tectonic rift extension to determine the hydrocarbon potential of the area.

Though a lot of work has been done in this area using different geophysical techniques mainly in geothermal prospecting, hydrothermal fluid studies, hydrochemistry and hydrogeology, no work has been done in mapping depocenters within the Magadi trough by use of gravity data. Through vision 2030 Kenya government hopes the country will be self-sufficient in affordable energy resources. There is need for more reliable sources of energy which will be sufficient for the growing population and industries. Reliable energy sources such as hydrocarbon, geothermal and coal are the major backbone of industrialization.

### 1.3 Location

Magadi trough is in the Kenya Tertiary rift, located about 110Km to the south of Nairobi. It is bounded by latitudes  $1^{\circ} 40' S$  and  $2^{\circ} 10' S$  and longitudes  $36^{\circ} 00' E$  and  $36^{\circ} 30' E$ . The area is located in the southern part of the Gregory Rift, an active continental rift that is part of the East African rift system whose formation is dated to early Miocene which was followed by volcanic activity in Turkana southwards. The Gregory Rift is of the continental type (Gregory, 1921). It extends from Lake Turkana in the north to Magadi-Natron basin in the south. The southern part of the Kenya rift is a region of geodynamic activity expressed by recent volcanism.

Lake Magadi is located in a broad flat depression that covers the lowest point in the southern Kenya Tertiary rift. Geothermal fields present in Magadi are characterised by fissure eruptions, which are trachytic in composition (Githinji et al., 2011). Magadi possesses the typical attributes of a rift valley basin in terms of hydrology, hydrochemistry and sedimentation, as well as the indices characterizing saline alkaline lakes: sodium carbonate evaporates or their pseudomorphs, Magadi-type chert, and tuffaceous rocks altered to zeolites and K-feldspar (Eugster, 1986).

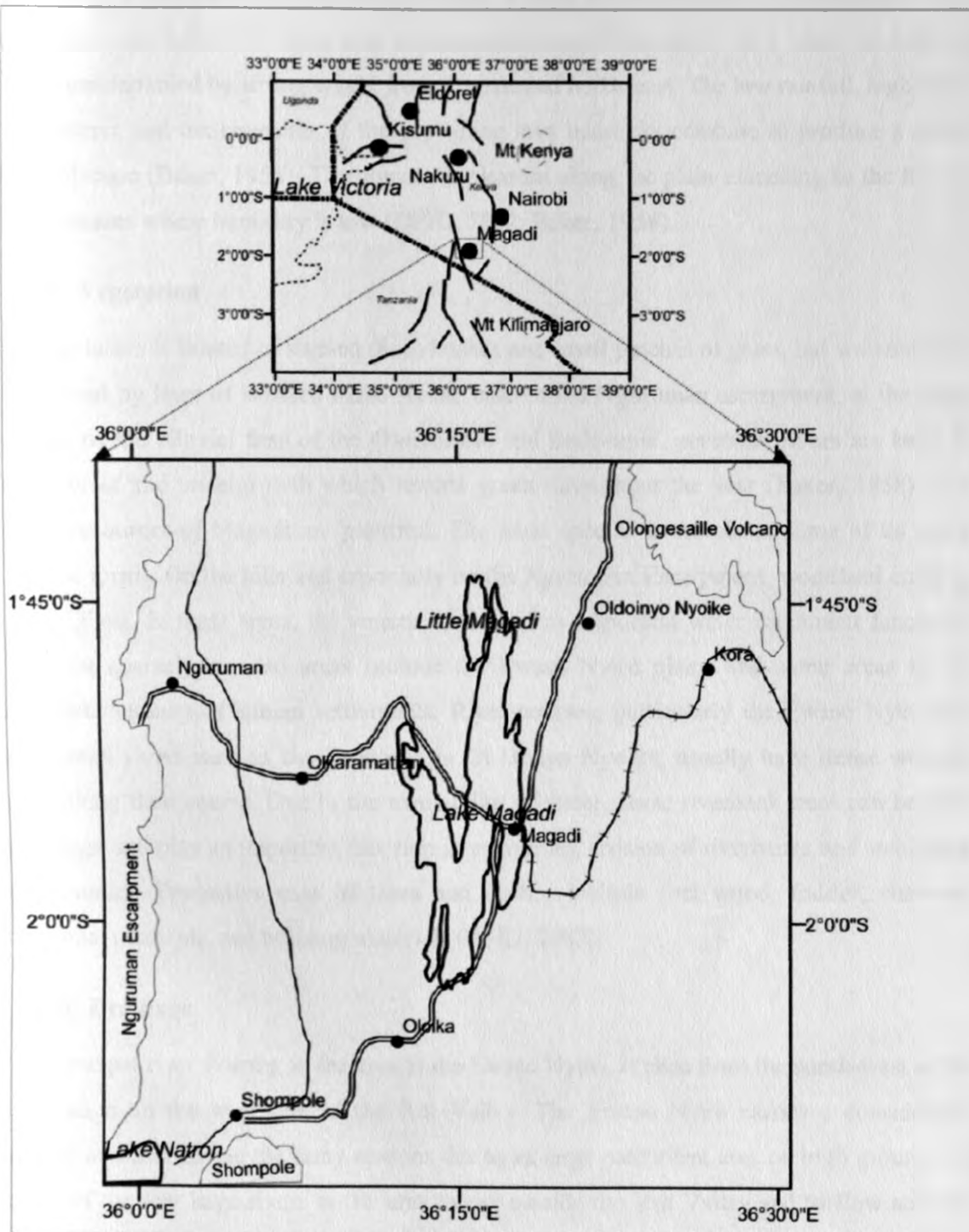


Figure 1.1: Location Map of study area (from Githinji et al., 2011)

## **1.4 Climate**

The climate is dry and hot as the rainfall is low. Almost all the rainfall is concentrated in two "rainy" seasons, March to April and in December, and often occurs as a result of isolated storms accompanied by strong winds from the east and north-east. The low rainfall, high daily temperatures and the character of the prevailing lava bedrocks combine to produce a semi-arid landscape (Baker, 1958). The climate is pleasant along the plain extending to the foot of the mountains where humidity is low (DFID, 2002; Baker, 1958).

## **1.5 Vegetation**

The vegetation is limited to stunted thorn bushes and small patches of grass, but watercourses are marked by lines of isolated trees. At the base of the Nguruman escarpment, at the outer margins of the alluvial fans of the Oloibortoto and Endosapia, perennial rivers are belts of dense forest and undergrowth which remain green throughout the year (Baker, 1958). The woody resources of Magadi are plentiful. The main species is Acacia in some of its many different forms. On the hills and especially on the Nguruman Escarpment, woodland cover is at its highest. In these areas, the vegetative cover has important water catchment functions. The most sparsely wooded areas include the Ewaso Nyiro plains and some areas in the immediate vicinity of human settlements. River courses, particularly the Ewaso Nyiro and other small rivers such as the Esonorua in Ol Donyo Nyoike, usually have dense wooded cover along their course. Due to the availability of water, some riverbank trees can become very large and play an important function in preventing erosion of riverbanks and stabilising watercourses. Productive uses of trees and bushes include fuel wood, fodder, charcoal, traditional medicine, and building materials (DFID, 2002).

## **1.6 Drainage**

The principal river flowing in the area is the Ewaso Nyiro. It rises from the south-west of the Mau range on the west side of the Rift Valley. The Ewaso Nyiro carries a considerable volume of water during the rainy seasons due to its large catchment area on high ground and is one of the few large rivers in the area to rise outside the Rift Valley and to flow and end here. Right bank perennial tributaries of the Ewaso Nyiro flowing off the Nguruman escarpment are (from north to south) the Longitoto, the Endosapia and the Oloibortoto rivers. The Longitoto river has spectacular falls some 107 m high at the point where it descends from the Naimithigirya plateau, while the Endosapia and Oloibortoto rivers have cut deep gorges into the escarpment and have many minor falls and rapids in their descent to the valley floor.

Only the Longitoto flows into the Ewaso Nyiro in the dry season; the others pass underground into their alluvial fans. Streams on the grid-faulted area are seasonal and consequent in character; they flow either into Lake Magadi or into small alluvium-filled basins of internal drainage caused by faulting.

### **1.7 Land Use and Land Resources**

Most of the land in Magadi area is used by pastoralists to graze their livestock. Most of the land is owned by group ranch members. The group ranches are primary based institutions that are responsible for common property management, while the income generating potential is based on the natural resources of the area, e.g., wildlife and breathtaking scenery (DFID, 2002).

The only cultivation in the area is found at the base of Nguruman escarpment, which is at the outer margin of the Oloibortoto and Endosapia perennial rivers. The Kalemma Wasonjo people, who inhabit the rest of the area use the Endosapia water in irrigating their fields. The Magadi Soda Company also has a small plantation irrigated by the waters of Oloibortoto River (Baker, 1958). Generally, Magadi area is about 97% arid and semi arid.

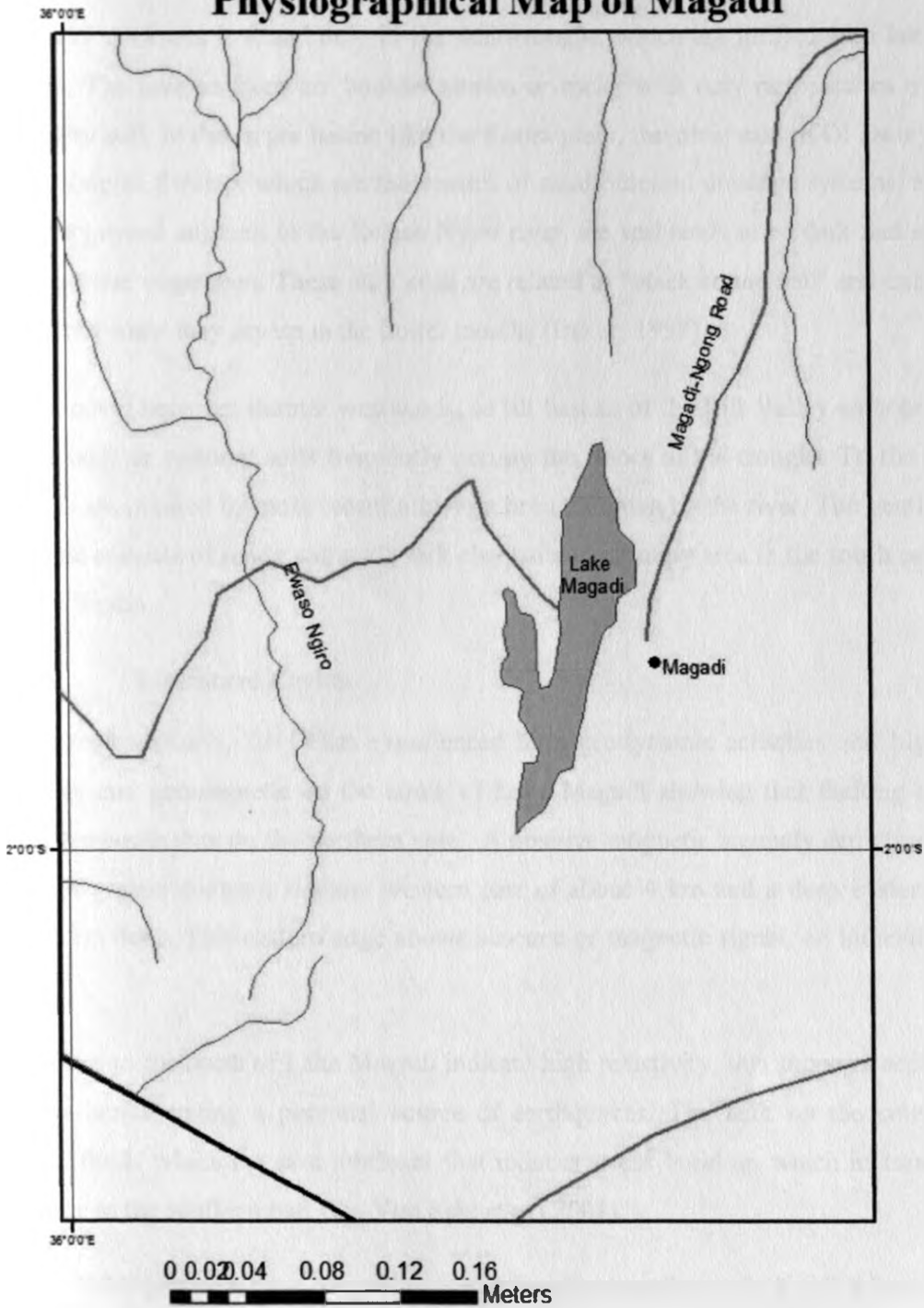
### **1.8 Physiography**

The area can be divided into three physiographic units, the mountainous country in the south east together with the gently-sloping soil pediment to the west of it, the central lava area consisting of many narrow horsts and troughs, and the Ngare Nyiro plain together with the southernmost and lowest part of the Nguruman escarpment. The central part of the area, which is composed of alkali trachyte and basalts, is closely grid-faulted along lines trending approximately 15 degrees east of north, the resulting topography being that of elongated ledges, platforms and troughs bounded by rocky escarpments which are generally vertical in the upper part. The Magadi trough traverses the area completely from north to south and it is bounded by fault escarpments. To the southern part of the trough, Lake Magadi is occupying the lowest part of the area being described. The Nguruman escarpment, which forms the western wall of the Rift Valley, descends to the east by moderate slopes from an altitude between 1828 m and 1981 m to a platform at about 1371 m, after which it drops spectacularly to the floor of the Valley. The upper part is clearly an old escarpment, consisting of deeply dissected Basement System rocks, while the lower scarp is young, precipitous, and relatively recently formed in volcanic rocks. Several perennial rivers that descend the escarpment have

built up alluvial cones of considerable size; some of these extend several kilometres from the base of the escarpment on to the valley floor. The Rift Valley floor is broken by a small fault escarpment. The floor of the valley declines southwards at a rate of approximately fifteen metres per mile and the "horsts" and "troughs" are similarly tilted (Baker, 1958). The major depressions in the Rift Valley floor from west to east are the Ewaso Nyiro valley, the Kordjya plain, the Magadi trough, the Koora plain and the Kwenia plain. The northern part of the Ewaso Nyiro depression is a tectonic basin through which the river flows in a deep gorge, while the lower part is the alluvial plain of the Ewaso Nyiro. The Kordjya plain, though not great in area, is the alluvium-filled plain formed by internal drainage into a fault basin on the lava surface (DFID, 2002).



# Physiographical Map of Magadi



## Legend

- Towns
- River
- International\_boundary
- Major Road
- Study Area
- L\_Magadi

Figure 1.2: Physiographical map of Magadi Basin

## 1.9 Soil

Soil of any thickness is found only in the fault-troughs, which are infilled with lake beds or alluvium. The lava surfaces are boulder strewn or rocky with only rare patches of yellow-brown silty soil. In the larger basins like the Koora plain, the plain east of Ol Doinyo Nyiro, and the Kwenia Swamp, which are the centres of small internal drainage systems, and in the low-lying ground adjacent to the Ewaso Nyiro river, the soil tends to be dark and supports a more luxuriant vegetation. These dark soils are related to "black cotton soil" and exhibit large deep cracks when they dry up in the hotter months (Baker, 1958).

The soil cover becomes thinner westwards, as till basalts of the Rift Valley emerges beneath it. Lake beds or swampy soils frequently occupy the floors of the troughs. To the north the lake beds are masked by more recent alluvium brought down by the river. The gently sloping sinu plane consists of sandy soil with dark clay soils in swampy area in the south eastern part of Njoro Sindio.

## 1.10 Literature Review

Magadi region (Kuria, 2011) has experienced high geodynamic activities and high rate of seismicity and geomagnetic on the south of Lake Magadi showing that faulting activity is high in the south than on the northern side. A positive magnetic anomaly depicting a 19 km wide half graben shows a shallow western part of about 4 km and a deep eastern edge of about 9 km deep. This eastern edge shows absence of magnetic signal, an indication of hot spring.

Fault zones to the north of Lake Magadi indicate high resistivity; this supports accumulation of stress hence setting a potential source of earthquakes. The fault on the southern part contains fluids which act as a lubricant that reduces stress build up which in turn, reduces seismicity in the southern part (Ibs-Von Seht et al., 2001).

Eugster (1986) recorded that Magadi possesses a typical attribute of rift valley basin in terms of its hydrology, hydrochemistry and sedimentation. The spring temperature in Magadi ranges from ambient to 86° C, and the total dissolved solids from 1000 to 3500 ppm. The recharge of the ground water system occurs through storm runoff and perennial streams descending the western part of the rift valley. A high pH environment results due to the production of authogenic minerals because of interaction of alkaline carbonate with volcanological sediments.



Akinola (2010) suggested that fault structures in the south of Lake Magadi serves as the fluid conduits which allow flow of hydrothermal fluid. The surface faults extend to a depth of 7.5 km into the subsurface. Fractures and faults are highly associated with brittle rocks within the crust and normally occur when the stress applied on the brittle rocks due to tectonics exceeds the elastic limit of the rock. The tectonics result due to the uprising of magma to the surface exerting pressure on the rock (Lerner and Cengage, 2003; Akiloni, 2010). The parallel faults bound the graben to the west and to the east. Magadi Curie depth point at a depth of 12.1 km marks the transition point between ductile and brittle crust, hence surface manifestation of the hot springs and high heat flow around Lake Magadi. Geodynamic activities in this area are as a result of correlation of the heat source, subsurface tectonic activities and seismic hypocenters (Molnar and Aggarwal, 1971; Ibs – von et al., 2001; Kuria et al., 2009 and Akinola, 2010). The systems of faults in Magadi area are as a result of the area being subjected to various tectonic activities (Jones et al., 1977; Maguire and Long, 1976; Lambiase, 1995).

Many of the minerals, especially the zeolites and cherts, provide a more permanent record of Magadi-type environments in geological record (Eugster, 1986). Sedimentation at Lake Magadi shows that the sub facies which are characterized by specific depositional processes and also providing building blocks for various depositional complexes are alluvial fans, sand flats, dry mudflats, saline mudflats, salt pans, perennial stream flood plains, ephemeral stream flood plains, spring deposits and shore line features. In Magadi trough itself alluvial fans are not common but magnificent fans are present on the western side of the rift valley where the perennial rim streams descend the 1500 m scarp formed by metamorphic rocks and basaltic flow. Sedimentary processes in closed basins are determined by climate, topography and nature of bedrock. Every sedimentary environment is characterized by specific depositional features. Reconstruction of the timing of diagenesis demonstrates that most of the processes occur soon after the deposition and are controlled by depositional environment and paleogeographical setting. The diagenesis of continental sediment is largely governed by the dynamics of ground water which, in turn, depend on geomorphology, climate and substrate character, e.g., compositions of the texture, porosity and permeability (Armeteros et al., 2010). At Magadi, sediment transport and deposition occur by ephemeral runoff and wind (Eugster, 1986).

Simiyu (1996) recorded that the upper most mantle structure has a density of  $3.18 \times 10^3 \text{ kg/m}^3$  in the Lake Turkana region and decreases to a minimum of  $3.12 \times 10^3 \text{ kg/m}^3$  beneath the Kenya dome in Lake Naivasha area. This density also increases to  $3.17 \times 10^3 \text{ kg/m}^3$  south of the apex of the Kenya dome at Lake Magadi implying possible low temperatures and less mantle plume upwelling than at the apex of the Kenya dome. High temperature to which the rock is subjected may alter geological structures and their contents (Levorsen, 1985).

The study in Yemen has shown that the occurrences of hydrocarbon are localized in a number of Mesozoic rift basins. The localization and tilt of these basins have an important influence in controlling hydrocarbon prospectively in the region (Hassan, et al. 2009) this Mesozoic basin was formed during two separate rifting events. Thus, the basin appeared to open from west to east with Marib basin dominated by Late Jurassic and Early Cretaceous fills followed by the Masila and Jiza' Qamar basins filling progressively with young sediments. The source and reservoir rocks were deposited as both pre- and syn-rift sediments, forming rift oriented traps during rifting within horsts and tilted fault blocks. The pools are sourced from Jurassic marine shales in adjacent down-faulted lows, which allow migration of hydrocarbon into the overlying and adjacent reservoir. The intrusion of deep-seated rocks into the overlying sediments may form a great variety of traps, including structural, stratigraphic and a combination of these. Some of these traps are associated with igneous rocks. Not all traps formed by intrusive rocks are productive; a great many unproductive traps have been formed in the sediments associated with the intrusions of salt as well as igneous rocks. Areal and linear fissures types of weathering crust are formed before overlapping of basement by rocks of the sedimentary cover. Areal crusts are pervasive at the basement roof, while linear fissure crusts are formed along fractures. The fissure type of eruption is common in the geothermal field of Magadi composed mainly of trachyte. Density modelling helps in understanding the structural interpretation within the areas covered by volcanics. It improves seismic interpretation, interpretation of the sub-basaltic sedimentary fill and the depth to the basement (Ashcroft et al., 1999; England et al., 2005; White et al., 2005).

Omenda (2007) records that the northern part of Lake Magadi indicates a region of geothermal prospect.

## 1.11 Justification and Significance

The primary goal of doing this study is to get a better understanding of subsurface geological structures. The gravity method is chosen for this study because it is a relatively cheap, non-invasive, non-destructive remote sensing method. It is also passive – that is, no energy is needed to be put into the ground for data acquisition; thus, the method is well suited for both populated and unpopulated setting. The small portable instrument used also permits walking traverses. Gravity measurements provide information about variations of rock densities in the subsurface; this assists the geoscientists to make inferences about the distribution of the subsurface composition in depth and size. The gravity method involves measuring the gravitational field strength exerted by the earth at a measurement station on the surface. The strength of the gravitational field is directly proportional to the mass of the body and therefore the density of subsurface materials. Anomalies in the earth's gravitational field result from lateral variations in the density of subsurface materials and the distance to these bodies from the measuring equipment (Marita, 2007). Gravity method guides other exploration methods such as seismic in delineating geological structures in the study area.

The study will be of more importance if depocenters can be mapped for this will lead to more investigation into their content. Depocenters are down warped region in the basement with high sediments accumulation. The reliable mapping of depocenters should increase more interest in the area in hydrocarbon exploration.

This project will be of great importance to the community around Magadi area and the country at large if the depocenters and structures are reliable to accommodate hydrocarbon. Since the communities staying in this area are pastoralist, the discoveries of hydrocarbon can be a boost to their way of living. The country will reduce its expenditure in importing the hydrocarbon and might also be a minor exporter or a major exporter depending on the amount of the deposits it may host to which this will generate foreign exchange to the country. International companies will also show interest in exploration of the trough and this may increase job opportunities

## **1.12 Aims and Objectives**

### **1.12.1 Aim**

The aim of this research is to map depocenters and subsurface geological structures within Magadi trough. Depocenters are down warped region in the basement with high sediments accumulation.

### **1.12.2 Specific Objective**

- a). To delineate geological structures using gravity anomalies.
- b). To determine depth to basement of the sediments within Magadi basin.

## CHAPTER TWO

### 2.0 GEOLOGY OF MAGADI

#### 2.1 Regional Geology

Magadi area consists of Precambrian metamorphic rocks, e.g., gneisses, quartzites and schists of the Turoka series. They are folded on the axes plunging gently to the north-east, and have suffered regional metamorphism and slight granitization. They contain such minerals as kyanite, garnet and graphite.

According to Baker (1958 and 1963), Sequar (2009), Atmaoui and Hollnack (2003), Magadi area is classified into three formations, namely Precambrian metamorphic rocks (the rocks include quartzite, gneisses, and chert), Plio-Pleistocene volcanics including alkali trachyte intrusion, and the Holocene to Recent lake and fluvial sediments. The Basement System rocks are confined to the upper slopes of the Nguruman escarpment where they form a dissected strike ridge. These rocks consist mainly of regular banded schists, gneisses and muscovite rich quartzites. The central volcanoes are three with Ologorsaile being the most important; the other two are Shompole and Lenderut volcanoes which are to the south of Magadi. Lenderut and Shompole are the closest central volcanoes in the area. Lenderut Volcano dated 2.5 million years (Ma) has basalt and andesite lavas, while Shompole dated 2.0 Ma consist of carbonatite and nephelinite rocks. In the southern and northern ends of Lake Magadi exists deposits of irregular interbedded chert rock composed of silicified banded clays on top of alkali trachyte.

There is no geological record of Palaeozoic or Mesozoic rocks in the area; the main period presented in the latter half of the Tertiary and the Quarternary when volcanicity, faulting, and later, lake and river sedimentation associated with rift valley took place. The Pleistocene basalts of eastern half of the area are younger than the Kirikiti basalts (Baker, 1958). The chert series principally outcrop in the vicinity of Lake Magadi. The chert beds invariably rest directly on the lava and are variable in both thickness and lithology. The sedimentary rocks are largely confined to the fault trough to the north of Magadi. This may be due to deposition in the troughs or due to their being down faulted and protected from erosion (Baker, 1958). Most of the large fault troughs in the area are floored by sediments, but it is comparatively rare that they are exposed. Sedimentary infillings of faulted troughs occur in Magadi area to the north (Baker, 1958). Lake Magadi-Natron is characterized by carbonatitic volcanism

(Simiyu, 1996). Numerous sub-parallel faults cut the Rift Valley floor and resulted in a general down faulting of the central strip which is now occupied by Lake Magadi.

Kuria (2011), Smith and Mosley (1993) record that the rift exists in the boundary between Tanzania Craton and Neo Proterozoic Mozambique belt is characterized by a complex fault zone

Bosworth et al., 1986 observed that there is a broad existence of a broad half graben depression and tilt block of late Miocene to Early Pliocene.

The rift system in which Magadi area is situated, evolved from asymmetrical graben to the east faced by half graben bounded to the west double system from normal fault (Le Gall et al., 2008).

According to Simiyu and Keller(1998) recording, the crustal structure of Lake Magadi has basement rocks at the bottom which are exposed to the western side of the Tanzania Craton, and the Mozambique belt to the eastern flank and overlain by Pliocene and Miocene volcanics and sedimentary rocks.

Period	Approx time 10 <sup>6</sup> year	Geological period	Type of processes				
			Tectonic activity	Volcanism	Sedimentation	Erosion	
Quaternary		Recent			sedimentation		Evaporite series, trona
						Erosion	Erosion
	0.1	Upper Pleistocene			sedimentation		High Magadi beds and Ewaso nyiro alluvium
			Tectonic activity			erosion	Minor faulting and erosion
	0.4	Midd. Pleistocene			sedimentation		Ologisalie lake beds and Cherts
	0.6		Tectonic activity			erosion	Grit faulting and erosion
					sedimentation		Oloronga Lake bed
				volcanism			Volcanic vents, ashes, scoria. Ol Doinyo Nyegi
			volcanism			Plateau trachyte	
	1	Lower Pleistocene		volcanism			Trachyte
Tertiary	2	Upper Pliocene	Tectonic activity			erosion	Nguruman fault II and erosion
				volcanism			Trachyte
				volcanism			Kirikiti basalt
				volcanism			Ologorsalie, Shompole and Lenderut Volcanics
	20	Midd / Lower Miocene	Tectonic activity			erosion	Nguruman fault I and erosion
						erosion	Erosion
Precambrian						Basement	

**Table 2-1: Geology of Magadi (modified from Baker, 1963)**

## 2.2 Geology of the Study Area

Geology of Lake Magadi area is characterized by Precambrian metamorphic rocks, the Plio-Pleistocene volcanics, and the Holocene to Recent lake and fluvial sediments. The Precambrian metamorphic rocks outcrop in the elevated west of Nguruman escarpment. These metamorphic rocks and olivine basalt of Kirikiti flat form and is down faulted to the rift floor at the Nguruman escarpment. Magadi plateau trachytes are closely followed by the development of ash and lava vent, and small obsidian lava cone. Oldoinyo Nyokie ends the volcanic formation of the southern Kenya rift. Lacustrine and fluvial sediments which include lake beds and fluvial sediments found in Ewaso Nyiro basin are recorded to form the last geological formation of Lake Magadi area (Kuria, 2011; Crossley, 1979).

The study area is bounded by Nguruman Escarpment consisting of Pliocene kirikiti basalt and Longitoto trachyte to the west, Lake Magadi to the east and Shompole and Lenderut volcano to the South. Ewaso Nyiro basin is covered with lacustrine sediments, alluvium, and ash. The area east of Shompole volcano and south west of Lenderut volcano is a plateau trachyte which crops into Tanzania.



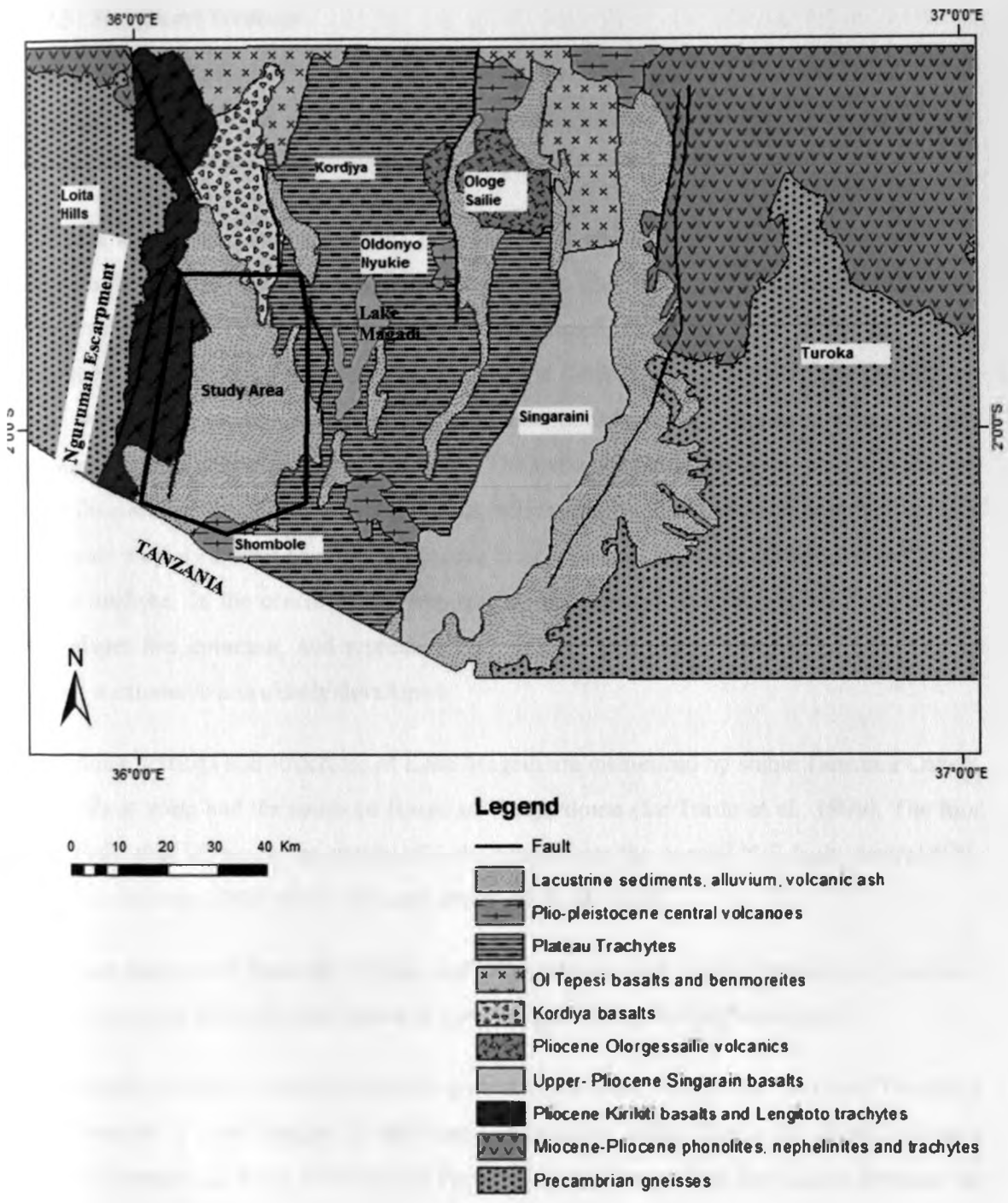


**Figure 2.1: Geological Map of Southern Part of Kenya Rift Valley (modified from Baker and Mitchell, 1976)**

Baker (1986) recorded that faulting increased immensely in the Magadi region from Pleistocene to Recent as can be compared to other segments of the Kenyan rift. Crustal thickness in the southern part is found to be 35 km where the axial zone is penetrated by feeder dykes originated probably from the upper mantle.

## CHAPTER THREE

### 3.0 GRAVITY METHODS

#### 3.1 Background

The gravity method was initially used in oil exploration for locating salt domes in the gulf coast of United States and Mexico and later for finding anticlinal structures in the mid continental area. In December, 1922, the Spindletop Oil Field initiated geophysical exploration by use of torsion balance. It is recorded that special types of structures in which hydrocarbon are trapped exhibit large contrasts in density with respect to the surrounding formations that the gravity data alone can be used to decide on the drilling locations. In north-western Peru, the oil entrapped by block faulting in shallow indurate formations was found by drilling guided by appropriate anomalies on gravity maps.

Most gravity surveys currently carried out in search for oil are designed for reconnaissance of large, previously unexploited areas. Where little or no geological information is available in a region, the first question that must be answered is whether the sedimentary region is large enough and thick enough to justify further investigation. If the geology is suitable, the gravity method can provide this kind of information rapidly and economically. Most sedimentary rocks have densities lower than basement rocks, and where this condition is met, the density contrast makes it possible to map the boundaries and determine the approximate depth distribution of sedimentary basins. Gravity surveys can be particularly useful in the initial exploration of water covered shelf areas, where no geological information may be available at all, and in extensive investigation of large- and medium-scale geological structures (Paterson and Reeves, 1985; Telford et al., 1990). It is used by the petroleum industry for the location of possible hydrocarbon traps, in microgravity engineering and archaeological survey like in such for cavities or bedrock which requires spacing of about 1 m.

In this project, subsurface geology was investigated on the basis of variations of the earth's gravitational field arising from difference in densities between subsurface rocks (Telford et al., 1990; Kearey et al., 2002). This concept is based on a causative body, which is a rock unit of different density from its surrounding. A causative body indicates anomalous mass and causes a localized perturbation in the gravitational field known as gravity anomaly. Local variations caused by rock densities near the surface causes very small changes in the gravity field. The prospecting by use of gravity has been employed as a secondary method in mineral

exploration for detailed follow up of magnetic and electromagnetic anomalies in the integrated base-metal survey

On small scale, buried relief on a bedrock surface like buried valley can give rise to measurable anomalies and on large scale, small negative anomalies are associated with salt dome, while major gravity anomalies are generated by granite plutons or sedimentary basins.

Gravity prospecting is also used as a reconnaissance tool in oil exploration. The data acquired are useful in providing constraints in seismic interpretation where the observation is made on the earth's surface.

This chapter outlines the principles and techniques used to achieve the objectives of this study.

## **3.2 Basic Theory**

### **3.2.1 Newton's Law**

The basis of the gravity survey method is Newton's law of gravitation, which states that the force of attraction between two particles of masses  $m_1$  and  $m_2$  is directly proportional to the product of the masses and inversely proportional to the square of the distance  $r$ , between the centres of the masses is given by

$$F = G \left( \frac{m_1 m_2}{r^2} \right) r_1 \quad 3.1$$

where  $F$  is the force on  $m_2$ ,  $r_1$  is a unit vector directed from  $m_2$  towards  $m_1$  and  $r$  is the distance between  $m_1$  and  $m_2$ . Where  $G$  is the universal constant.

#### **3.2.1.1 Acceleration of Gravity**

Force is related to mass by acceleration and the term  $g = GM/R^2$  is known as the gravitational acceleration or, simply, gravity. The weight of the mass is given by  $mg$ . On such an Earth, gravity would be constant. However, the Earth's ellipsoidal shape, rotation, irregular surface relief and internal mass distribution cause gravity to vary over its surface (Kearey et al., 2002)

Acceleration  $g$  of mass  $m_2$  due to the presence of mass  $m_1$  is given by

$$g = G \left( \frac{m_1}{r^2} \right) r_1. \quad 3.2$$

If  $m_1$  is the mass of the Earth,  $M_e$ ,  $g$  becomes the acceleration of gravity and is given by

$$g = G \left( \frac{M_e}{R_e^2} \right) r_1 \quad 3.3$$

$g$  is measured in mGal.

Where  $R_e$  is the Earth radius and  $r_1$  is a vector that extends downwards to the centre of the Earth.

The gravitational field is most usefully defined in terms of the gravitational potential  $U$ :

$$U = \frac{GM}{r} \quad 3.4$$

Whereas the gravitational acceleration  $g$  is a vector quantity, having magnitude and direction (vertically downwards), the gravitational potential  $U$  is a scalar, having magnitude only. The first derivative of  $U$  in any direction gives the component of gravity in that direction. Consequently, a potential field approach provides computational flexibility. Equipotential surfaces can be defined on which  $U$  is constant. The sea-level surface, or geoid is the most easily recognized equipotential surface, which is everywhere at right angles to the direction of gravity.

### 3.2.1.2 The gravity units

The mean value of gravity on the Earth's surface is approximated to be  $9.8 \text{ m/s}^2$ . The gravity variation caused by subsurface density variations in the subsurface are in the order of  $100 \mu\text{m/s}^2$ . The micrometer per Second Square is referred to as the gravity unit (gu). The c.g.s unit of gravity is the milligal ( $1 \text{ mGal} = 10^{-3} \text{ Gal} = 10^{-3} \text{ cm/s}^2 = 10 \text{ gu}$ ).

In gravity measurement, absolute gravity values at survey stations may be obtained by reference to the International Gravity Standardization Network (IGSN) of 1971, a network of stations at which the absolute values of gravity have been determined by reference to sites of absolute gravity measurements. By using a relative reading instrument to determine the difference in gravity between an IGSN station and a field location the absolute value of gravity at that location can be determined.

### 3.2.1.3 Gravitational potential

#### a). Newtonian or three dimensional potential

Gravitational fields are conservative. The force giving rise to a conservative field may be derived from a scalar potential function  $U(x, y, z)$ , called the Newtonian or three dimensional potential

$$\nabla U(x, y, z) = -g(x, y, z) \quad 3.5$$

Where  $g$  is the gravitational acceleration,

$$g = \left(G \frac{m}{r^2}\right) \mathbf{r}_1 \quad 3.6$$

$$\nabla U(x, y, z) = -G \frac{m}{r^2}(x, y, z) \quad 3.7$$

Where  $m$  is the mass of the geological body

$$m = \rho dv \quad 3.8$$

where  $\rho$  is density of the geological body and  $dv$  is the elementary volume of the geological body.

$$dv = dx dy dz \quad 3.9$$

$$\nabla U(x, y, z) = -G \rho \frac{dx dy dz}{r^2} \quad 3.10$$

Where  $r^2(x, y, z) = x^2 + y^2 + z^2$

$$r(x, y, z) = \sqrt{x^2 + y^2 + z^2} \quad 3.11$$

$$U(r) = \int_{\infty}^r m \left(\frac{1}{r^2}\right) dr = G \frac{m}{r}$$

$$dU = G \frac{m}{r} = G \rho \frac{dx dy dz}{r} \quad 3.12$$

$$\sum \nabla U(r^{\wedge}) = \int du dr = \int \frac{G \rho dx dy dz}{(\sqrt{x^2 + y^2 + z^2})} \quad 3.13$$

Where  $r^{\wedge}$  is a vector

The gravitational potential U of whole 3D body of arbitrary shape is given by

$$U = G\rho \iiint_{xyz} \frac{dx dy dz}{\sqrt{x^2+y^2+z^2}} \quad 3.14$$

$$\text{If } U(t) = G\rho \iiint \frac{1}{r} dx dy dz \quad 3.15$$

U(t) is gravitational potential at t

r is the distance between t and point mass dm (dx dy dz)

G is the gravitational potential

$\rho$  is the density of geological body

The derivative of the potential with respect to the vertical axis (z component) leads to gravity effect. Thus if g is the acceleration in the z direction then

$$g = - \left( \frac{\partial u}{\partial z} \right) \quad 3.16$$

by replacing the value of equation 3.14 into equation 3.16 yield

$$g = G\rho \iiint_{xyz} \frac{z}{r^3} dx dy dz \quad 3.17$$

equation 3.13 is the gravity effect which result from gravitational potential U

using cylindrical coordinate  $dx dy dz = r \cdot dr \cdot d\theta dz$ , the potential becomes

$$U = G\rho \iiint_{r,\theta,z} \left( \frac{r_z}{r} \right) dr \cdot d\theta dz . \quad 3.18$$

And the acceleration in Z direction becomes

$$g = G\rho \iiint_{r,\theta,z} \left( \frac{r_z}{r^3} \right) dr \cdot d\theta dz \quad 3.19$$

In spherical coordinates,  $dx dy dz = r^2 \sin\theta dr d\theta d\phi$  gravitational acceleration becomes

$$g = - G\rho \iiint_{r,\theta,\phi} \left( \frac{z}{r} \right) \sin\theta dr d\theta d\phi \quad 3.20$$

From equation 3.15 potential of the spherical coordinates become

$$U = G\rho \iiint_{r,\theta,\phi} r \sin\theta dr d\theta d\phi \quad 3.21$$

**b). Logarithmic or two dimensional potential**

If a body is very long, say in y direction and its x and z dimensions can be determined, its gravity attraction can easily be derived from logarithmic potential and its gravity effect becomes

$$U = G\rho \iint_{xz} dx dz \int_{-\infty}^{\infty} \frac{dy}{r} \quad 3.22$$

$$r = (x^2 + y^2 + z^2)^{1/2} \quad 3.23$$

From 3.22 the integral part from  $\pm\infty$  can be written as  $\int_{-\infty}^{\infty} \frac{dy}{(x^2+y^2+z^2)^{1/2}}$

If  $\pm\infty$  is replaced by a finite length t and let t approach infinity then

$$\int_{-\infty}^{\infty} \frac{dy}{r} = \int_{-t}^t \frac{dy}{(x^2+y^2+z^2)^{1/2}} = \int_{-t}^t \frac{dy}{(a^2+y^2)^{1/2}} = u_t \quad 3.24$$

Where  $a^2 = x^2 + z^2$

Using the relation  $\int \frac{f'(x)}{f(x)} = \ln f(x) + C \quad 3.25$

Where  $f'(x) = \frac{df(x)}{dx} \quad 3.26$

And  $\int \frac{dy}{x^2+y^2} = \ln \left[ \frac{y+(y^2+x^2)^{1/2}}{x} \right]$

then  $u_t = \int_{-t}^t \frac{dy}{(a^2+y^2)^{1/2}} = \ln \left[ \frac{t+(t^2+a^2)^{1/2}}{-t+(t^2+a^2)^{1/2}} \right] \quad 3.27$

if t goes to infinity, we obtain

$$u_t = \ln\left(\frac{2}{a^2} \times \frac{1}{2}\right) = -2 \ln r$$

Using the mathematical relation of equation 3.8, the logarithmic or two-dimensional potential becomes:



$$U = 2G\rho \iint_{xx} \ln\left(\frac{1}{r}\right) dx dz \quad 3.28.$$

The gravity effect for a two dimensional body then becomes

$$g = -\left(\frac{\partial u}{\partial z}\right) = 2G \iint_{xx} \rho \left(\frac{z}{r}\right) dx dz \quad 3.29$$

#### 3.2.1.4 Potential field equation

Potential in free space satisfies Laplace's equation,  $\nabla^2 U = 0$  and, in Cartesian coordinates, is given by

$$\nabla^2 U = \frac{\partial^2 U}{\partial x^2} + \frac{\partial^2 U}{\partial y^2} + \frac{\partial^2 U}{\partial z^2} = 0 \quad 3.30$$

A very small volume  $V$  enclosing point mass results to Poisson's equation

$$\nabla^2 U = 4G\pi\rho \quad 3.31$$

Gravity potential satisfies both Laplace's equation in free space and Poisson's equation in the region containing mass.

### 3.2.2 Three Dimensional Euler deconvolution

The deconvolution is the most popular technique used to interpret potential field data in terms of simple sources characterized by the value of the degree of homogeneity. It is usually applied to data at a constant level (Tatiana, 2009). Euler deconvolution is sensitive to error both in anomaly amplitude resolution and in determination of vertical and horizontal gradient which are highly sensitive to noise (Steenland, 1968). The quality of the depth estimation in Euler deconvolution depends mainly on the choice of the proper structural index which is a function of the geometry of the causative bodies. Euler deconvolution uses the magnetic or gravity field and its three orthogonal gradients (two horizontal and one vertical) to compute for anomaly source location along X, Y, and Z direction, by choosing an appropriate square window size, that is applied to the data grid of total potential field and three derivatives, setting structural index and uncertainty of solutions, then finally solving  $X_0$ ,  $Y_0$  and  $Z_0$  within the window (Keating and Pilkington, 2004; Dewangen et al., 2007). The window moves throughout the whole data grid. Window size is a function of grid cell and must be set in such a way that it includes large variations but does not skip small details.

Marson and Klingele (1993) have shown the advantages of using the vertical gradient of gravity for Euler deconvolution of gravity data. They solved Euler's equation in a moving window, over only areas that contain the maxima of the amplitude of the analytic signal or of the horizontal derivative, in which choice of the optimum structural index was based on the standard error of the solutions and their clustering.

Structural index which relates to source type (e.g, contacts, dike, and point) is set by considering geological knowledge of the survey area as well as structure that interpreter is tending to represent. Majid (2010) showed that the standard Euler deconvolution uses three orthogonal gradient of any potential quantity to locate a source body. Theoretically, the gravity and magnetic field caused only by pure 2D and 3D sources satisfy Euler homogeneity equation exactly. Euler deconvolution and analytical signal are both used for semi-automatic interpretation of potential field data, they are used to delineate contacts and obtain rapid source depth estimation of geological structures (Fairhead and Green, 1994; Zhaofang, 1994; Reid et al., 1990; Petar, 1997; Keating and Pilkington, 2004). So it is an important method because depth and shape estimates can be obtained without the need for data on the vector of density contrast of the source. The equation of Euler's homogeneity relation is written as:

$$(X-X_0)\frac{\partial T}{\partial x} + (Y-Y_0)\frac{\partial T}{\partial y} + (z-z_0)\frac{\partial T}{\partial z} = N (B - T) \quad 3.32$$

where T is the observed potential field at (X, Y, Z)

$X_0$ ,  $Y_0$  and  $Z_0$  are the unknown coordinates of the source body centre or source to be estimated, X, Y and Z are known coordinates of the observation points of the gravity and the gradients  $\frac{\partial T}{\partial x}$ ,  $\frac{\partial T}{\partial y}$  and  $\frac{\partial T}{\partial z}$  are the first derivatives in x,y and z directions.

B denotes the base level of the observed field or "regional" field within a sliding window with adjustable size. N denotes the structural index which is a measure of the rate of change with distance of a field.  $X_0$ ,  $Y_0$ ,  $Z_0$  and B are unknowns parameters.

According to Changyou et al. (2000) equation 3.32 will be

$$(X-X_0)T_{xx} + (Y-Y_0)T_{yy} + (z-z_0)T_{zz} = N (B_z - T_z) \quad 3.33$$

For the gravity anomaly vertical component  $T_z$  of a body having a homogeneous field and where  $T_x, T_y, T_z$  are the measured gravity gradients along the  $x, y$  and  $z$  directions. This equation 3.33 can be written as

$$X_0 T_{zx} + Y_0 T_{zy} + Z_0 T_{zz} + NB_z = XT_{zx} + YT_{zy} + ZT_{zz} + NT_z \quad 3.34$$

The values of unknowns can be worked out metrically.

According to Stavrev and Reid (2007) the degree of homogeneity (structural index) depends on the type and physical parameter of the potential field. Equation 3.33 can be solved in a window centred on a given grid point to find unknown source point  $(X_0, Y_0, Z_0)$  and the regional field (Reid et al., 1990). This approach introduces nonlinear relation between the structural index and unknown regional field. By specifying structural index, Euler equation is solved using a linear least square method (Majid, 2010).

Many potentials of simple isolated gravity or magnetic source (point mass, point dipole, line-mass, line-dipole) have the general form (Thompson 1982):

$$T(x, y, z) = G/\rho^N \quad 3.35$$

$\rho = ((x - x_0)^2 + (y - y_0)^2 + (z - z_0)^2)^{1/2}$  is the distance and  $G$  is a constant. In this case  $T(x, y, z, x_0, y_0, z_0)$  is homogeneous of structural index  $N = -n$ .

Using a moving window of a selected size along the profile, an over-determined system is solved and one solution  $(x_0, y_0, z_0, N)$  is obtained for each position of the window. In the theoretical case the solution is unique but in the real data interpretation. The presence of noise or the interference due to other sources causes some scattering of the solutions around the true value. Equation 3.35 is valid at each point belonging to the harmonic region and therefore along vertical or oblique profiles connecting points located at different altitudes in the upward-continued field. In particular, Euler's equation applied to the points of every straight line passing through the source position assumes the form

$$\rho \cdot \nabla f = (x - x_0) \frac{df}{dx} = (y - y_0) \frac{df}{dy} = (z - z_0) \frac{df}{dz} = nf \quad 3.36$$

Equation 3.36 represents the basic relation, which allows estimations of the unknown source coordinates  $(x_0, y_0, z_0)$  and degree of homogeneity  $n$ .

The structural index can be determined by observing the clustering of the solutions for different structural index values; for a particular feature, the correct structural index yield a tighter cluster. The degree of homogeneity of the gravity field is  $n = 1$  for a contact or for a fault of large thickness but for a thin fault or semi-infinite thin plate the degree of homogeneity is  $n = 0$  (Petar, 1997; Stavrev and Reid 2007). Geometrical type of the physical parameters can be specified by an index  $n$ , so that  $n=0$  for quantities of point masses or moments and  $n = 1, 2$ , and  $3$  for line, surface and volume densities of the point masses or moments respectively. Reid et al (1990) and Thompson (1982) recorded structural index ( $n$ ) value corresponding to magnetics structures as follows:  $n = 0$  for contacts,  $n = 0.5$  for fault,  $n=1$  for sill/dyke,  $n=2$  for pipe,  $n=3$  for sphere.

### 3.2.3 Analytical signal

Analytical signal is a quantity which can be calculated either in space or frequency domain and its amplitude is independent to magnetization direction (Ansari et al., 2009).

Analytical signal is applied in determination of source parameter, in which quantities related to analytical signals and the vertical potential gradient is required. The structural indices are simply one greater when using analytical data (and its three orthogonal derivatives). Taking derivative to calculate analytical signal effectively remove the (unknown) background or case level field  $B$  in equation 3.32. Absolute value of analytical signal is the square root of the sum square of vertical and two horizontal derivatives of a potential field (Nabighan et al., 2005). The analytical signal indicates maximum contrast. Location of maxima shows the outlines of gravity sources. The analytical signal method, when applied to observed gravity data, produces good horizontal locations for the contacts and sheet sources no matter the geological dip.

For the case of 3D the analytical signal (Roest et al., 1992) is given by

$$\mathbf{A}(x,y) = \frac{\partial T}{\partial x} \mathbf{i} + \frac{\partial T}{\partial y} \mathbf{j} + \frac{\partial T}{\partial z} \mathbf{k} \quad 3.37$$

where  $\mathbf{i}$ ,  $\mathbf{j}$ ,  $\mathbf{k}$  are unit vectors in  $x$ ,  $y$ ,  $z$  directions and  $T$  is the potential field. From equation 3 the amplitude of the analytical signal in 3D case is given by

$$|\mathbf{A}(x,y)| = \sqrt{\left(\frac{\partial T}{\partial x}\right)^2 + \left(\frac{\partial T}{\partial y}\right)^2 + \left(\frac{\partial T}{\partial z}\right)^2} \quad 3.38$$

Intrusive bodies (mafic and ultramafic intrusions) in sedimentary section can be interpreted by use of interactive forward modelling, inversion methods (Barbosa and Silvia, 2011). In this study Euler deconvolution and analytical signal techniques were used in the interpretation of the gravity data.

### 3.2.4 Horizontal gradient of gravity

The horizontal gradient is determined from gravity contour maps as the slope or rate of change of gravitational acceleration (g) with horizontal displacement (Telford et al, 1990). Gravity data are often useful in defining lateral extent of geological bodies such as plutons or sediments filled valleys, when the data is subjected to horizontal derivative technique. Horizontal gradient gravity provides a simple and rapid way of viewing data from a very different perspective (Dobrin and Savit, 1988).

Horizontal gradient of gravity is given by

$$U_{xz} = - \frac{\partial g}{\partial x} = 3G\rho \iiint_{xyz} \left(\frac{xz}{r^5}\right) dx dy dz \quad 3.39$$

### 3.2.5 Upward continuation

The transformation of gravity data measured on one surface to some higher surface is called upward continuation.

Upward continuation is a physical smoothing method based on the Laplace's equation. Upward and downward continuation applies harmonic functions because they naturally define their space behaviour. Upward continuation is a filter operation that tends to smooth the original data by attenuating short wavelength anomalies relative to their longer wavelength counterparts, a logical consequence of the attenuation of anomaly amplitude with increasing distance from the source. The opposite approach of downward continuation through hopefully homogeneous layers enhances the small-scale local features. In the spectral domain, the amplitudes vary exponentially, as  $e^{kz}$ , with the vertical z and the wave number k (where z < 0 upward). Upward continuation filter  $F_2(k_x, k_y)$  is elegantly simple for special case of a data measured on a flat surface

$$F_2(k_x, k_y) = e^{-kz} \quad (k = (k_x^2 + k_y^2)^{1/2}) \quad 3.40$$

The equation 3.40 shows that as we move away from the source, all wave numbers are attenuated by  $\exp(-kz)$  and the highest wave numbers (short wavelengths) are attenuated most rapidly. Therefore upward continuation can be seen as a very smooth, low pass filter.

As with standard low pass filters, upward continuation often provides perspective concerning the large regional source beneath a study area, but it's simple physical interpretation (this is how gravity data would look if they had been measured on the higher surface) sometimes offers a definite advantage over the application of low pass filters with less obvious physical significances. Anomalies with short wavelengths in the original data are attenuated relative to anomalies with larger dimensions by upward-continuation filter (Dobrin and Savit, 1988). Many of the remaining features are caused by source of more regional scale.

### 3.2.6 Vertical derivative

The first-order vertical derivative of the gravity field at each height is calculated in the space domain using the method of finite differences proposed by Florio et al., (2006). It also has the advantage of allowing the calculation of vertical derivative at several heights, using a stable operator like upward continuation (Jacobsen, 1987). Using forward differences, the vertical derivative of the gravity field  $g$  at the height  $h$ , is defined as

$$g_{vd} = \left(\frac{\partial g}{\partial z}\right)_h = \frac{g_{uph+\Delta h} - g_{uph}}{\Delta h} \quad 3.41$$

where  $g_{uph}$  is the field upward continued at the height  $h$ ,  $g_{uph+\Delta h}$  is the field upward continued at a slightly higher level  $h+\Delta h$ , and  $\Delta h$  is a small height difference lying between 1/10 and 1/100 of the data sampling interval. Conventionally, the vertical derivative should be assigned to an altitude of  $h + \Delta h/2$ , but since  $\Delta h$  is so small, vertical derivative can be set to level  $h$  (Florio et al., 2006).

Vertical derivative enhance shallow anomaly much more than deeper anomalies and gives a better resolution of closely spaced sources.

## 3.3 Interpretation methods

Interpretation method involve qualitative and quantitative interpretations

### 3.3.1 Qualitative Interpretation

Qualitative interpretation is an important step of making conscious choices of the range of possible models, better than being unconsciously guided by preconceived ideas. It is essential for determining the direction of the search for probable mass distributions that cause the observed gravity anomalies (Wolfgang, 2009). Quantitative interpretation involves determination of shapes, trends, locations and densities of anomalies by close examination of their characteristic features. Gravity anomalies can be estimated for bodies or structures that

are likely to be encountered by guessing their size, shape and density contrasts and approximating them by simple geometrical shapes (Dobrin and Savit, 1988). Contours are commonly used in identifying structures. Steepness of a geological body is identified by closely tight contours while sudden change in contours is an indication of depth discontinuity, likely a fault.

### **3.3.2 Quantitative Interpretation**

In quantitative gravity interpretation, the locations, depths, shapes and density contrasts of geological bodies are to be defined as accurately as possible. This is done by numerical calculation using computer program. It may be desirable to first isolate those parts of the observed gravity anomalies which are caused by the target bodies, and this is part of interpretation. The whole task, thus, will be to approach the truth by combining all available information and adjust it mutually within the error limits of each. The compromise between all pieces of conflicting evidence is largely a matter of judgement and experience.

Gravity interpretation is never final: any new data warrant better quantifying the models. Another valuable aspect of gravity interpretation is its suitability to aid interpolation between gaps in other types of information, for example, between boreholes or seismic surveys. Standard methods as seismic reflection may also leave blind spots where gravity modelling can be applied profitably to fill such gaps. Thus, gravity is and remains a unique and economic tool for exploration.

Non-ambiguous quantitative information, contained in gravity anomalies, is the total amount of the anomalous mass and its horizontal centre of gravity. The accuracy of the information depends on the accuracy of the data and, to a large extent, on the definition of the zero level of an investigated anomaly. In a somewhat similar fashion, maximum depths may also be estimated. Downward continuation of gravity anomalies through homogeneous layers can also give some direct insights by computing the idealized mass anomaly in the form of the equivalent stratum, but it is only a guide to quantitative interpretation.

Quantifying the error bounds is an essential aspect of quantitative interpretation.

The mathematical approach to this problem is optimization and inversion. It is the last step to arrive at quantitative models and their uncertainties by matching the gravity observations and

adjusting the model parameters that generate the matching effects. It is not an aspect of gravity alone, but also of any other a priori information.

### 3.3.3 Direct and Indirect Methods

Direct and indirect methods are also known as forward and inverse modelling methods respectively. These methods are involved in quantitative interpretation. An interpretation method is called direct if some parameters describing a model (e.g. density, dimensions, location, depth, etc.) are calculated directly from characteristic features of the observed anomaly,  $\delta g(x)$  (e.g. amplitude, "half width", some ratios, etc.) by the use of formulae or diagrams or "characteristic curves". Such direct methods are based on rather simple models with only few parameters. Otherwise the direct relation between observation and model parameters will not be direct. Some of the direct methods belong into the category of estimates or quick semi-quantitative methods (Kearey et al., 2002)

The indirect approach is the traditional trial and error procedure. It is iterative and starts with assuming a preliminary or initial model, calculating its effects,  $\delta g_m$ , and continues with comparing them to the observations,  $\delta g_{obs}$ . The residual field ( $r_i$  or  $r = \delta g_{obs} - \delta g_m$ ) is then examined for systematic space variations which may be, again, interpreted by modifications to the previous model, i.e., taken to estimate the model changes (or the difference model) which lead to reduce the residuals or to better fit the observations. This is repeated until the fit is considered satisfactory. The aim is to match the observed anomalies by the computed effects; however, it suffices within the error bounds of the observations.

The final residuals are (from the original observed data) considered small enough and their variation is considered sufficiently random in space. If trial and error is carried out manually, it is guided mainly by experience. By it one finds an acceptable model, i.e., one that is compatible with the observations, but not all variants which are also data-compatible. This must be considered within the geological constraints. Indirect interpretation by trial and error cannot be standardized for the determination of depth, shape and density of 3D mass anomalies.



## CHAPTER FOUR

### 4.0 DATA ACQUISITION AND PROCESSING

#### 4.1 Data Acquisition

##### 4.1.0. Introduction

Gravity data is acquired in the field by use of gravimeter on a profile or on a grid. Before any data is acquired the base station is set which is revisited after 3 to 4 hours to check for the drift of the gravimeter. It is necessary to use the same station for checking drift because any station can be reoccupied. The correction of the drifting effect is done after acquisition of data in that survey. The spacing of stations where the data is collected or where the gravimeter is read for data acquisition is to be fixed along a profile or in a grid. The station spacing used in a gravity survey may vary from a few meters in the case of detailed mineral or geotechnical surveys to several kilometres in regional reconnaissance surveys.

The spacing in the mineral exploration is different from spacing in oil exploration. In oil exploration, a more or less uniform grid of the station is desirable. Stations 0.5 to 1 km apart on loops roughly 6×6 km in size might be typical for petroleum survey because the structures associated with oil accumulation are large.

##### 4.1.1. Data source

The data used in this study was acquired by National Oil Corporation of Kenya (NOCK) in 1974 in Magadi area. Gravimeter LaCoste Romberg G-16 of precision 0.01 Mgal, was used in raw data acquisition in irregular grid. The measurement was done in the field by levelling gravimeter precisely for station readings, in which extra care and time was observed to obtain acceptable measurements. An average spacing of 2 km was maintained. Vehicle odometer was used to maintain the distances and to reduce inaccuracy between stations.

The station density was greatest where the gravity field was changing most rapidly. Where absolute gravity values were required in order to interface the results with other gravity surveys, at least one easily accessible base station was available where the absolute value of gravity was known. During gravity survey, the gravimeter was read at a base station at a frequency dependent on the drift characteristics of the instrument. At each survey station, location, time, elevation and gravimeter reading were recorded. Gravity meter was read to a precision of  $\pm 0.01$  mGal in order to reduce gravity value accurate to  $\pm 1$  gu. The latitude of

the station was known to  $\pm 10$  m and elevation of the station was known to  $\pm 10$  mm. The latitude of the station was determined on 1:50000 maps. The highly accurate elevation measurements were determined barometrically using a barometer.

Gravity stations coordinates were determined by global positioning system (GPS).

## **4.2 Preliminary Data Acquisition**

The study involved reviewing of previous work in the area and other related areas of study. This involved reading through electronic journals with information related to the study from a broad perspective, progressive reports of the study area and theses of those who have done similar studies.

The following were some of the materials and tools used in carrying out this study

- a). Personal computer (laptop): where computers software's b) to e) below were stored and interpretation operated.
- b). Spread sheet: Microsoft Excel for filing data in XYZ file.
- c). Word processor: Microsoft Word 2007 for word processing
- d). Arc GIS : Arc map Sri 2010 for locating the station position and digitizing geological map
- e). Geosoft Oasis Montaj 6.4.2. (2007) for data interpretation.

### **4.2.1 Gravity Instrument**

Gravimeter is the instrument which is heavily used in gravity prospecting; the instruments which have been used before the advent of the gravimeter are the torsion balance and the pendulum. There are several types of gravity meters which have been employed in gravity geophysics prospecting and, these are:

- a) Stable-type gravimeter. It is very sensitive to other physical effects like change in temperature, pressure, and small magnetic and seismic variations.
- b) Unstable type gravimeters. They are more sensitive than stable meters because of their state of unstable equilibrium
- c) LaCoste-Romberg gravimeter

d) Worden gravimeter

The gravimeter is used in acquiring gravity data in the field at different station points.

The data used for this study was acquired by NOCK, on land, by use of LaCoste Romberg gravimeter G-16. The data from the study area were extracted from gravity database kept by National Oil Corporation of Kenya (NOCK). Below is a type of LaCoste Romberg gravimeter used in gravity data acquisition.

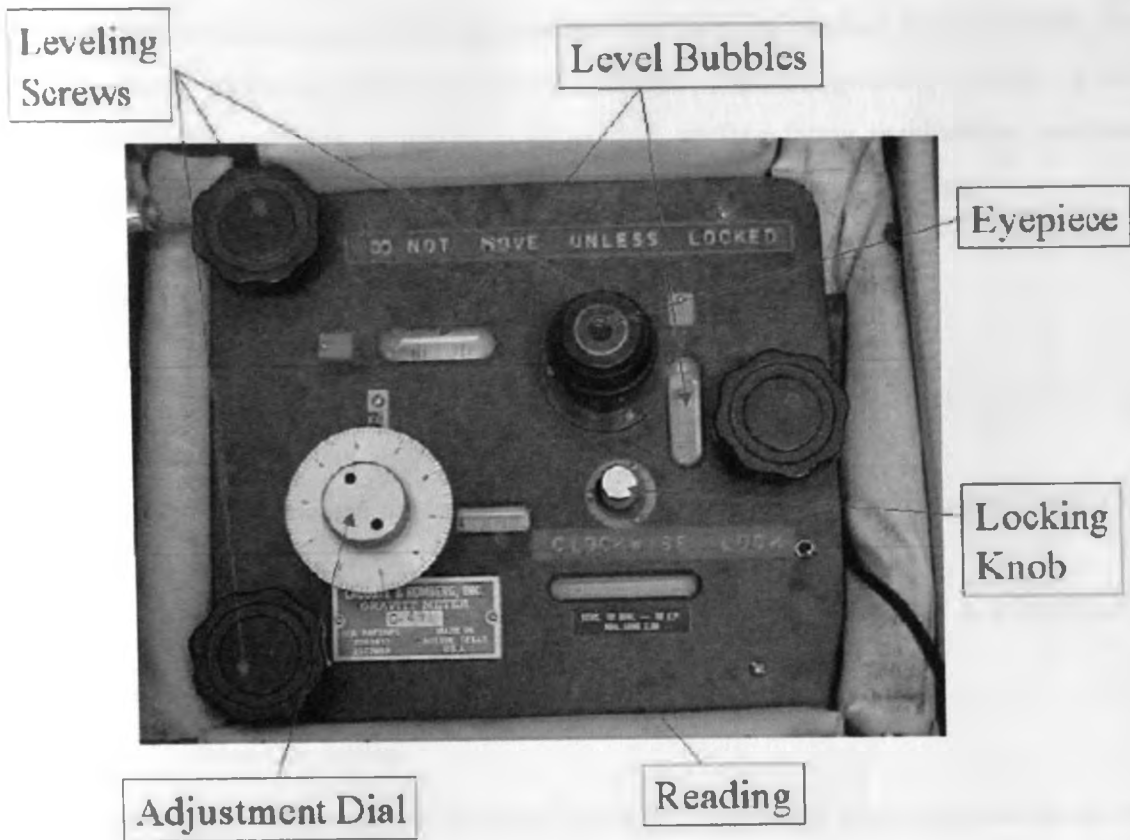


Figure 4.1: LaCoste and Romberg gravimeter

### **4.3. Data Processing**

#### **4.3.1 Introduction**

Geophysical surveys measure the variation of some physical quantity, with respect either to position or to time. The geophysicist's task in data processing is to separate signals from the noise and interpret the signals.

In processing gravity data, the effects of shallow masses of short wavelength are removed by filtering out (smoothing) short wavelength anomalies. The effects of deep wavelength are called regional. Residual gravity is obtained when the regional and near surface noises have been removed; residual presumably represent effects of the intermediate zone of interest. The data processing methods applied in gravity includes empirical gridding method, second vertical derivative methods, graphical residualizing, surface-fitting residualizing methods, field continuation (upward and downward continuations), wavelength filtering.

The following were undertaken when gravity data was being processed:

- a. Conversion from dial divisions to mGal.
- b. Determination of the instrumental drift and applying the corrections to the observed data
- c. calculation and applying corrections to the gravity values measured during the survey
- d. Plotting the corrected data (which is the Bouguer anomaly) as a function of distance.

#### **4.3.2 Data Correction**

Gravity readings are influenced by latitude, elevation, topography of the surrounding station, earth tides and density variation in the subsurface.

Before the results of gravity survey can be interpreted, it is necessary to correct for all variations in the Earth's gravitational field, which do not result from the differences of density in the underlying rocks. This process is known as gravity reduction or reduction to the geoid, as sea-level is usually the most convenient datum level. Drift correction, Latitude correction, Terrain correction, Free air correction and Bouguer corrections are the gravity reduction methods which were used to correct the field data. The complete Bouguer anomaly was achieved after these corrections.

#### 4.3.2.1 Drift Correction

The drift correction was done by repeating readings at base station, at a recorded time throughout the survey. The meter reading was plotted against the time. The drift was mainly due to creeping in the spring. The reading at the base station was repeated after 2 hours. After drift correction, the difference in gravity between an observation point and the base station was determined. This was done by multiplying the difference in meter reading by the calibration factor of the gravimeter. The absolute gravity at the observation point  $g_{obs}$  was computed from known value of gravimeter at the base station.

#### 4.3.2.2 Latitude Correction

Gravity varies with latitude because of the non-spherical shape of the Earth, and because the angular velocity of a point on the Earth's surface, decreases from a maximum at the equator to zero at the poles. The centripetal acceleration generated by this rotation, has a negative radial component that consequently causes gravity to decrease from pole to equator. Points near the equator are farther from the centre of mass of the Earth, than those near the poles, causing gravity to increase from the equator to the poles. The amplitude of this effect is reduced by the differing subsurface mass distributions resulting from the equatorial bulge; the mass underlying equatorial regions being greater than that underlying Polar Regions. The net effect of these various factors is that, gravity at the poles exceeds gravity at the equator by some 51860 gu, with the north-south gravity gradient at latitude  $\phi$  being  $8.12 \sin 2\phi$  gu km<sup>-1</sup>. Latitude correction was done by subtracting the predicted gravity at latitude  $\phi$  i.e.  $g\phi$  which is the predicted value of gravity at sea level, at any point on the earth's surface from the observed gravity ( $g_{obs}$ )

$$g\phi = 9780318.5 (1 + 0.005278895 \sin^2 \phi + 0.000023462 \sin^4 2\phi) \text{ mGal} \quad 4.1$$

#### 4.3.2.3 Elevation Corrections

Free air and Bouguer corrections fall under elevation corrections.

##### a). Free Air Correction

The free-air correction (FAC) correction was done to correct for the decrease in gravity with height. Free air results from increased distance from the centre of the Earth (Kearey et al, 2002).

$$\text{FAC} = 3.086h \text{ gu (h in metres)} \quad 4.2$$

Free air correction is normally added to the field reading where the station is above the datum plane. Since the study area was above datum plane the free air readings were added to the field readings.

It is important to note that for latitude and free-air corrections, station positions must be known precisely.

### b). Bouguer Correction

The Bouguer correction (BC) was done to account for the attraction of materials between the station and the datum plane, which was ignored in free air calculation.

$$BC=2\pi G\rho h =0.4191\rho h \text{ gu (h is in metres, } \rho \text{ in mg/m}^3\text{)} \quad 4.3$$

The Bouguer correction was subtracted from station reading, because the gravitational attraction of the rock between the observation points and datum must be removed from the observed gravity value. The main effect of Bouguer correction is to remove large gravity differences between nearby points at different elevations. Bouguer correction was applied in the opposite sense to free air. Since elevation of the study area was above sea level, the Bouguer correction values were subtracted from the observed gravity data values.

#### 4.3.2.4 Terrain Correction

Terrain correction allows for surface irregularities in the vicinity of station. Hill above the elevation of the gravity station exerts an upward pull on the gravity, while valleys below it, because of lack of materials fails to pull downward on it. The terrain correction was added to the station reading.

Calculations of the terrain reading require detailed knowledge of relief near the station. In areas of steep and erratic slopes it is not very accurate particularly for relief in the vicinity of the station itself. At the edge of steep cliff or gorge, the terrain correction is almost inevitable in error. A better solution was achieved by moving gravity station away from sharp relief features where it was possible.

## ity Anomaly

uced generated gravity anomaly. Gravity anomalies are conventionally or as contour maps. Interpretation of the latter may be facilitated by use essing technique (Telford and Geldart, 1990).

es employed on data used for this study are Complete Bouguer Anomaly, and Simple Bouguer Anomaly.

### Complete Bouguer Anomaly

ie Bouguer gravity anomaly the following element were considered:

- a) The expected increase in gravity in latitude this is the latitude effect ( $g_{lat}$ ).
- b) The expected decrease in gravity with increasing elevation above sea level or datum level this is the free air effect ( $g_{fe}$ ).
- c) The expected increase in gravitational attraction due to mass of rock at sea level or datum and the observation point this is the Bouguer effect ( $g_{Boug}$ ).

r Anomaly (CBA) was obtained after data correction. It formed the basis of mplete Bouguer Anomaly was obtained after; latitude correction, free air er correction and terrain correction were added or subtracted from the shown in the equation below

$$CBA = g_{ob} - g_t + (\Delta g_L + \Delta g_f - \Delta g_b + \Delta g_T) \quad 4.4$$

tation reading,  $g_t$  is the theoretical gravity,  $\Delta g_L$  is the latitude correction,  $\Delta g_f$  rection,  $\Delta g_b$  is the Bouguer correction,  $\Delta g_T$  is the terrain correction (Telford

### Free Air Anomaly (FAA)

model include prediction of theoretical gravity on a reference surface, and for the fact that the gravitational attraction decreases as the observations are ove sea level a reference surface (Dobrin and Savit, 1988).

$$FAA = g_{ob} - g_0 + FAC (\pm EC) \quad 4.5$$

Where  $g_{\theta}$  is the predicted value of gravity at latitude  $\theta$ , FAC is the free air correction, BC is the Bouguer correction, TC is the terrain correction (Kearey et al, 2002).

### 4.3.3.3 Simple Bouguer Anomaly (SBA)

Simple Bouguer anomaly was calculation by subtracting from the FAA, the effect of the infinite horizontal slab of thickness equals to the stations height (h) and density of 2.67 g/cm<sup>3</sup>. Thus

$$\text{SBA} = \text{FAA} - 2\pi G\rho h = \text{FAA} - 0.1119h \text{ (in mGal)} \quad 4.6$$

The complete Bouguer anomaly computed is not much different from the Simple Bouguer Anomaly, as height (h) changes involved is not large.

This study was carried out with the use of gravity data, which was acquired from National Oil Corporation of Kenya (NOCK), from an already existing data set in a complete processed form. The reduction of data to Bouguer anomaly value was done by density of 2.69 g/cm<sup>3</sup>. Various gravity data reduction techniques such as Bouguer correction, free air correction and terrain correction was applied in which Free air anomaly (FAA), Simple Bouguer anomaly (SBA) and Complete Bouguer anomaly (CBA) were obtained.

From the data set stored by NOCK, 66 data points were extracted covering the study area. Specific lines L1 and L3 were identified on the data set covering the entire study area on the map of Magadi. All station numbers corresponding to L1 and L3 were recorded from the data set. The coordinates of station number positions corresponding to those recorded from the data set was found using Arc GIS on the map, in latitude and longitude. The coordinates of station numbers in latitude and longitude were recorded down on a note book. This information assisted in extracting the data corresponding to each station numbers from the data set in terms of grid east, reference north in km, free air anomaly (FAA), Terrain correction, Simple Bouguer Anomaly (SBA) and Complete Bouguer Anomaly (CBA). The culmination of the data acquisition was marked by presenting processed data in xyz file, visualizing and interpretation of the results.

The accurate interpretation of the data was aided by a priori information of the area geology section 2.2. The approach to the interpretation of gravity anomalies was to approximate the geological feature considered to be the source of the body. This was done by assigning a



simple geometrical form, for which the gravity field could be computed mathematically (Dobrin and Savit, 1988).

Geosoft Oasis Montaj was used in processing gravity data. The completed Bouguer anomaly map was obtained where data in xyz format was gridded, and then contoured using Oasis Montaj version 6.4.2. Oasis Montaj contain several techniques which were employed in production of other different Maps for this study. The techniques which were employed are the upward continuation, analytical signal, horizontal derivative, vertical derivative and 3D Euler deconvolution and the resulting maps are shown in figures 5.1, 5.2, 5.3, 5.4, 5.5, 5.6,.

The following are the stages which were involved in processing gravity data obtained from NOCK:

- Converting data to data files
- Arranging data files into XYZ format
- Plotting gravity anomaly map using Oasis Montaj.

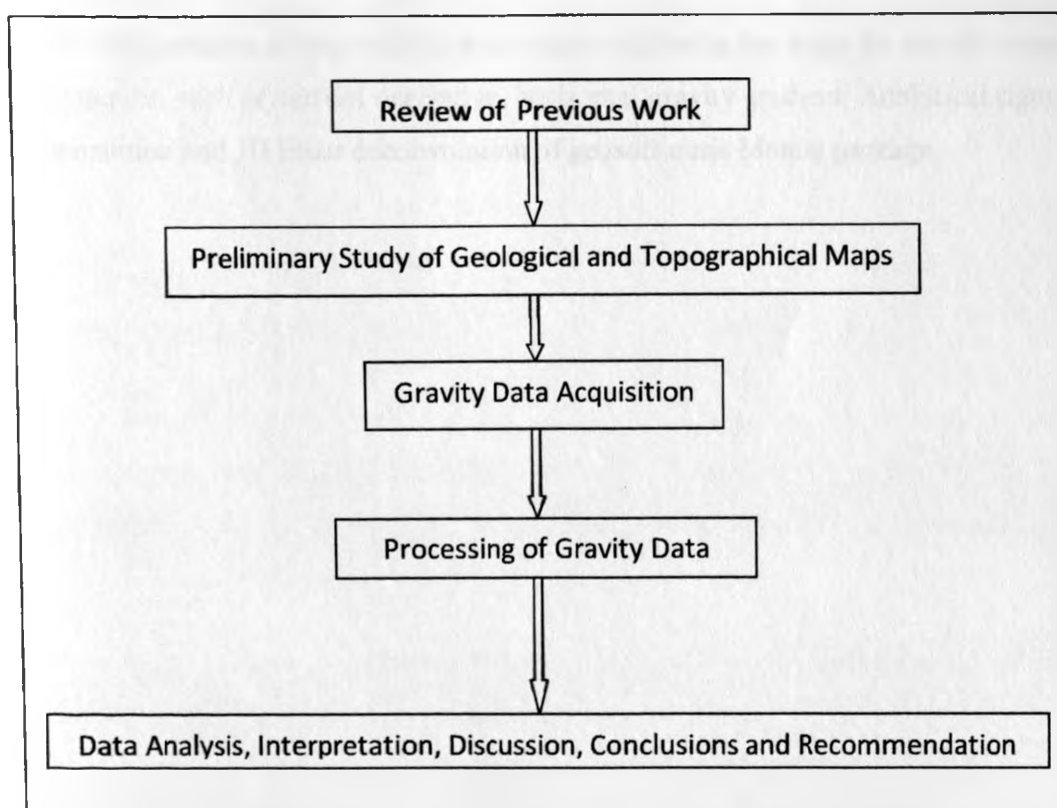


Figure 4.2: Schematic diagram illustrating the methodology

## **CHAPTER FIVE**

### **5.0. DATA INTERPRETATION, RESULTS AND DISCUSSION**

#### **5.1. Introduction**

Interpretation will allow an assessment to be made about the depth and size of the causative body. Interpretation of anomalies is the inverse problem with the aid of forward solutions. The interpretation problem is finding the mass distribution responsible for the residual anomaly. Interpretation of gravity data is done by comparing the shapes and sizes of the anomalies to those caused by bodies of various geometrical shapes at different depth and densities (Gadalla and Fisher 2009; Kearey et al, 2002).

The gravitational field strength is vital for mapping sedimentary basin, since it depends mainly on the density contrast of the anomalous body beneath the subsurface. The cause of variations in gravitational field can be determined, and this will also assist in determining the source depth which affects the field gravity. By so doing, the thickness of sediments to basement can easily be determined, because the distance to basement will be a clear indicator of the source depth.

The effective interpretation of gravity data was made possible in this study by use of various filtering techniques, such as vertical derivative, horizontal gravity gradient, Analytical signal, upward continuation and 3D Euler deconvolution of geosoft oasis Montaj package.

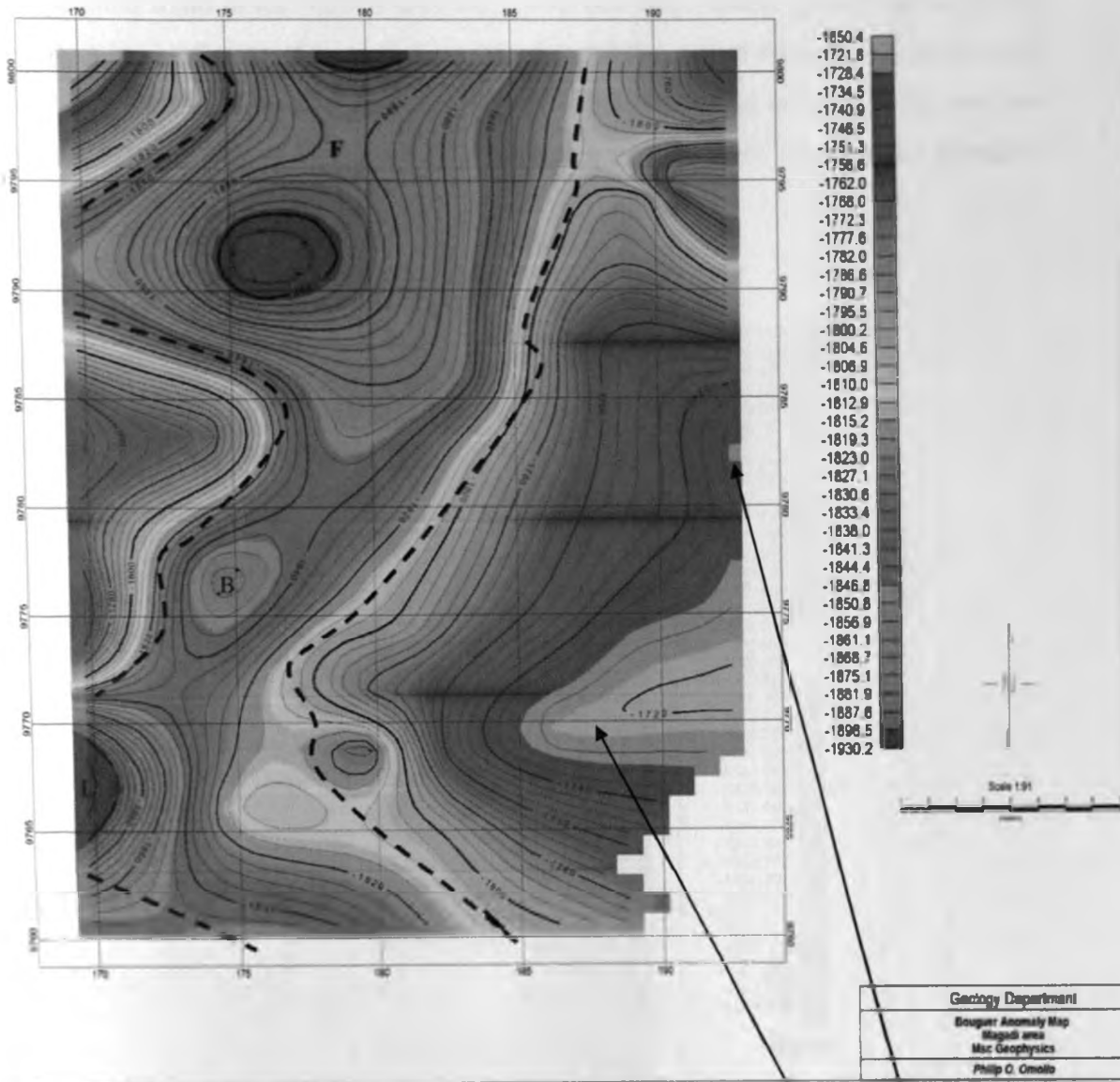


Figure 5.1: Complete Bouguer Anomaly Map

Dyke Dyke

The observed Bouguer anomaly was the sum of long and short wavelength components normally caused by deep seated and near-surface geological bodies, respectively. The gravitational effect of causative bodies, at two different source horizons, was estimated from the regional and residual components of the Bouguer data.

Bouguer anomaly map shows the influence of both shallow and regional structures, and their varying depth of burial. The response of shallow and deep structures of acquired gravity data, results to complete Bouguer Anomaly map obtained. The hot (red and orange) colour and the cold colour (blue and green) exhibit gravity high and gravity low respectively. The map shows that the anomalies trend in the NE-SW. Anomalies of low gravitational field intensity

form a specified trend in the NE-SW direction, with two large lowest gravity value (marked F) forming a basin like structure to the north, and a similar one to these two is to the south (marked L) and are bounded by anomalies of high gravitational field intensity to the west and to the east. The dotted black lines in the map show regions of low gravity anomalies demarcating fault lines trending in NE-SW and NW-SE direction.

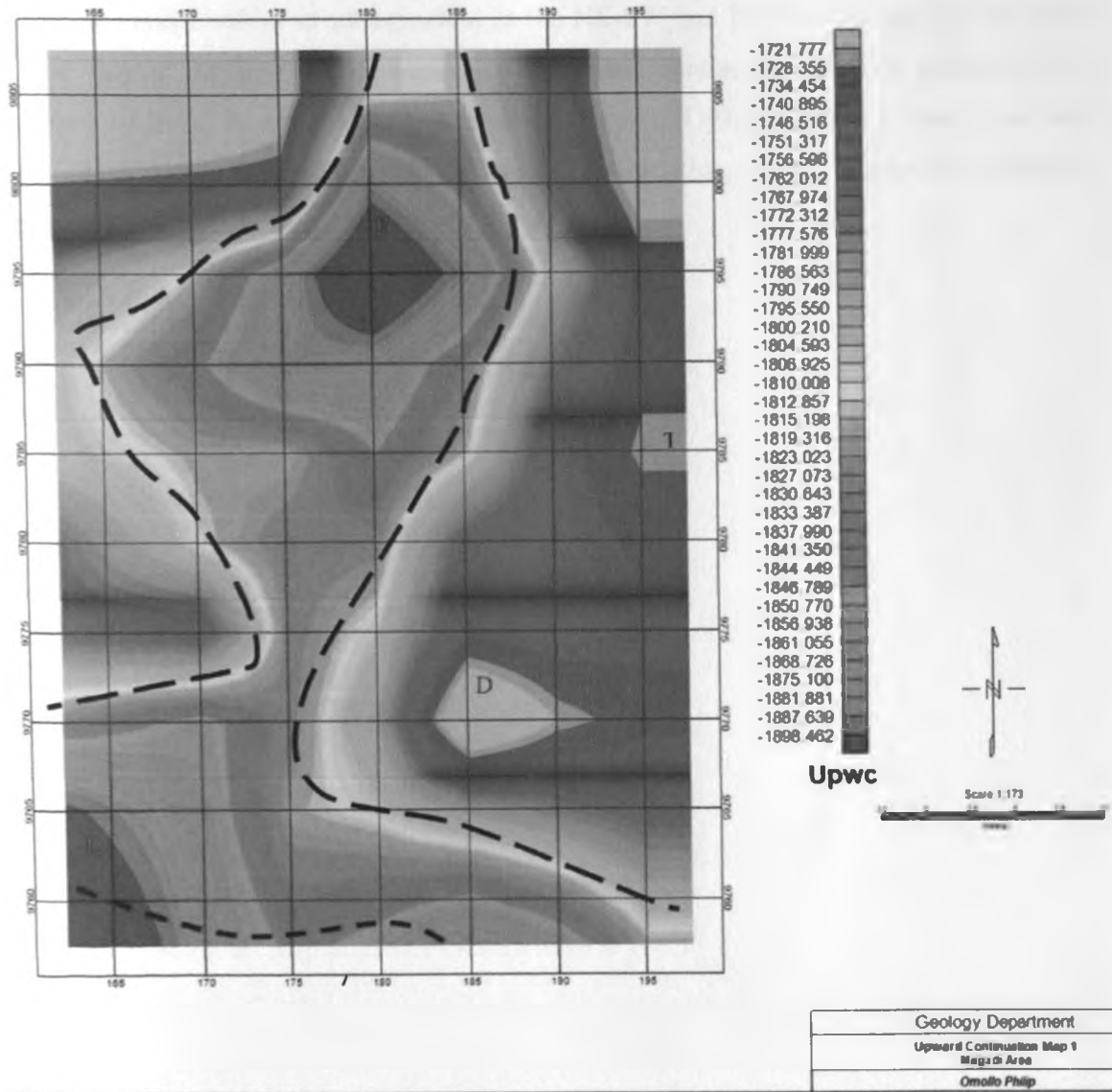


**Figure 5.2: Upward Continuation map Continued at 1 km using a grid cells size of 5**

In comparing the upward continuation map and complete Bouguer anomaly map, it is evident that upward continuation technique is best in suppressing the near surface anomalies, and enhances the regional anomalies or deep seated anomalies. The bodies with high gravity values between -1790 mGal to -1722 mGal on the eastern and western side of the map can be

interpreted as intrusive bodies. The anomalous bodies with the lowest gravity values of about -1898 mGal to -1850 mGal, is bounded by other bodies of low gravity value of about -1844 mGal to -1812 mGal to the northern and southern part of the study area. These areas of lowest gravity values in the map, can be said to be centres of high sediment accumulation, and are the depocenters indicated by letters F, B and L in figures 5.1. Depocenters are down warped region in the basement with high sediments accumulation. The map also shows that the regional and residual structures trend in the NE-SW and NW-SE. As depicted in figure 5.2, the shapes and sizes of the anomalies in upward continuation map, is smaller in size compared to those in complete Bouguer anomaly map. Dykes labelled D and T are well exhibited in the upward continuation map, this shows that upward continuation enhance regional anomalies and attenuate the shallow anomalies.

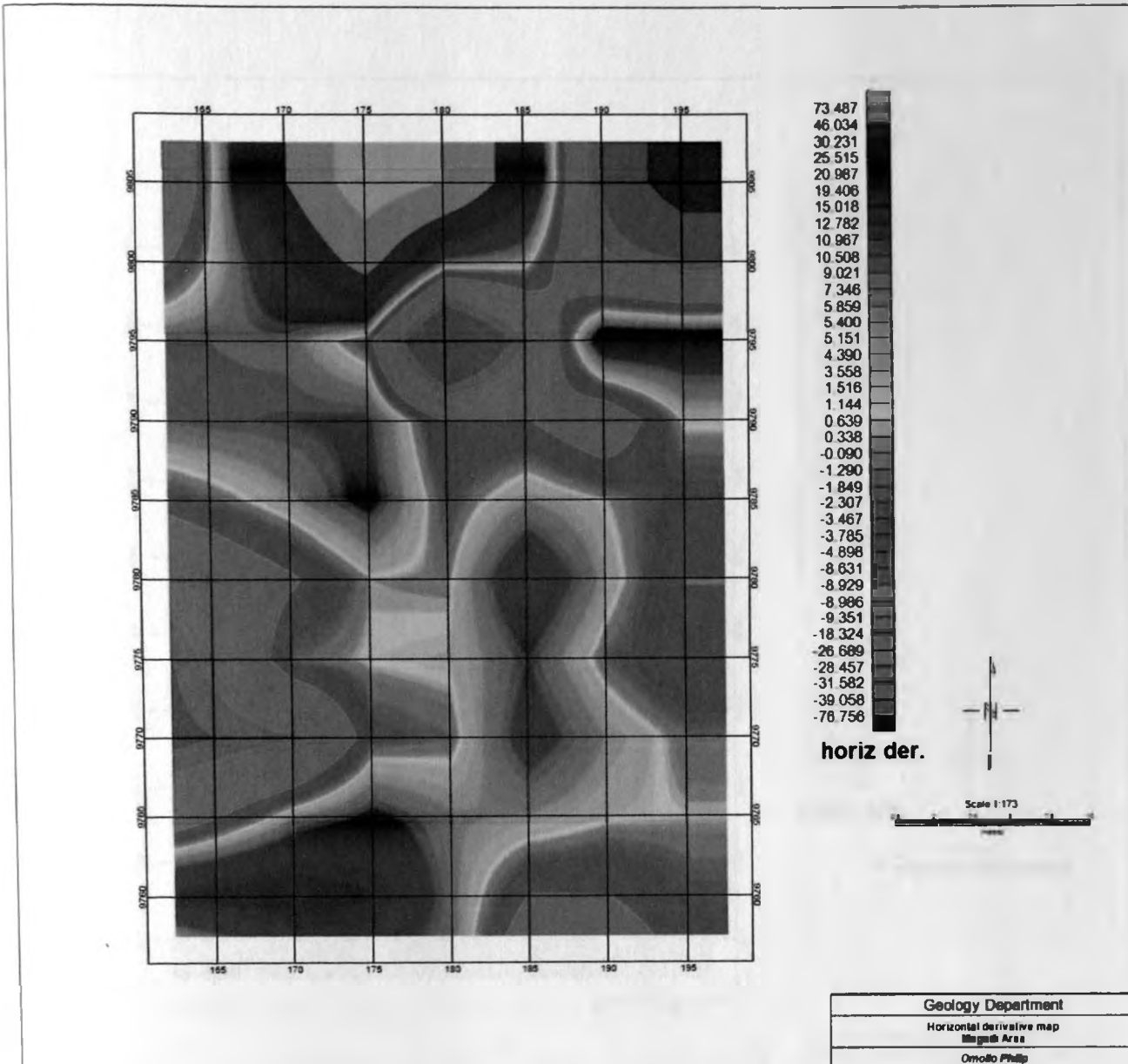


**Figure 5.3 : Horizontal Derivative Map of first order of grid cell size 5**

The maximum value of the horizontal gravity gradient, tend to be located on the horizontal edges of the gravity sources is marked by rapid change in density values (Blakely, 1996).

Horizontal derivative therefore, provides a simple and rapid way of viewing the data from a very different perspective. The derivative defines the lateral edge of the subsurface bodies. The map shows the effectiveness of horizontal derivative in delineating the structures boundaries in the study area. The derivatives are strongest mostly on the north western and south western part (figure 5.3).

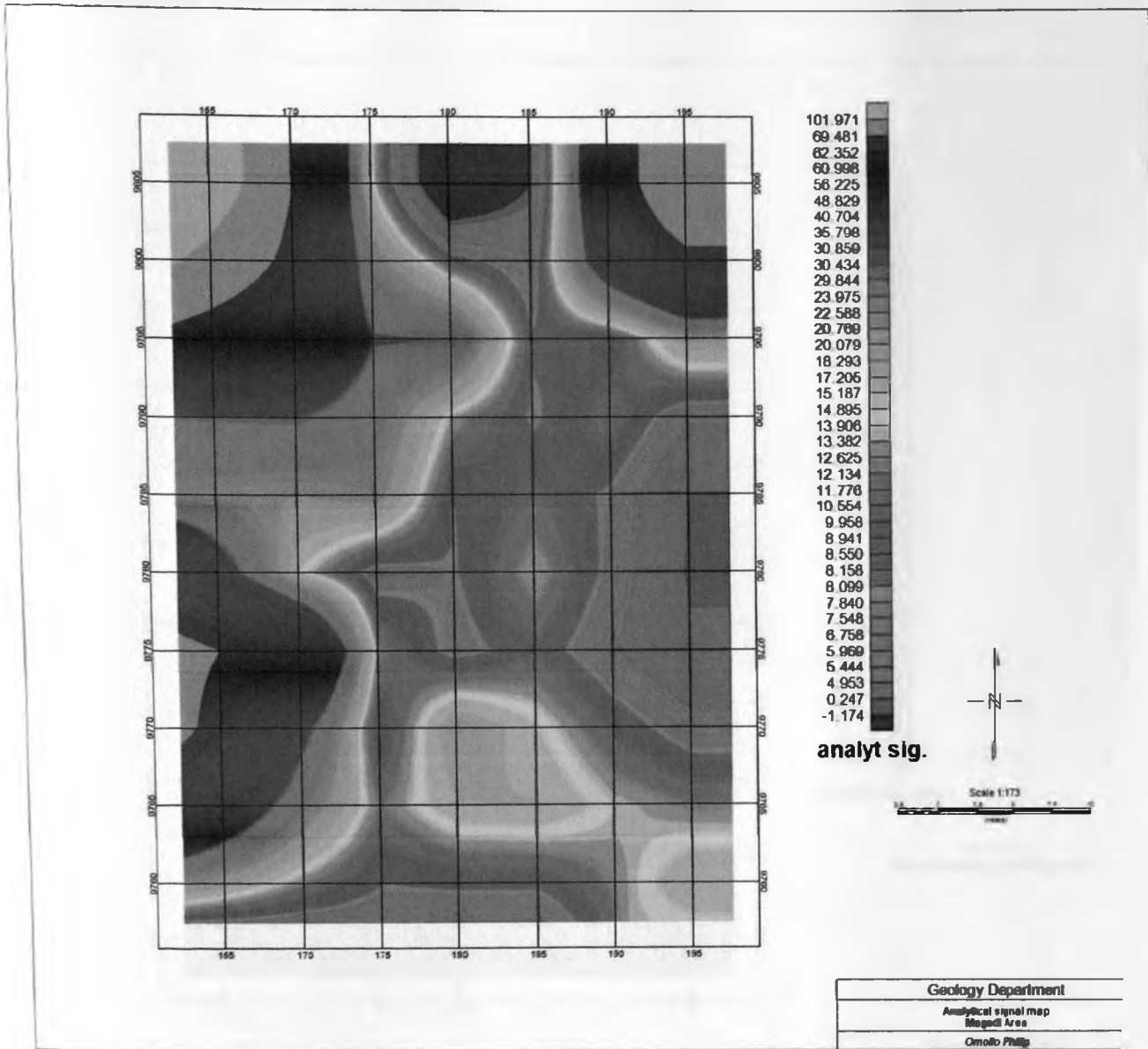
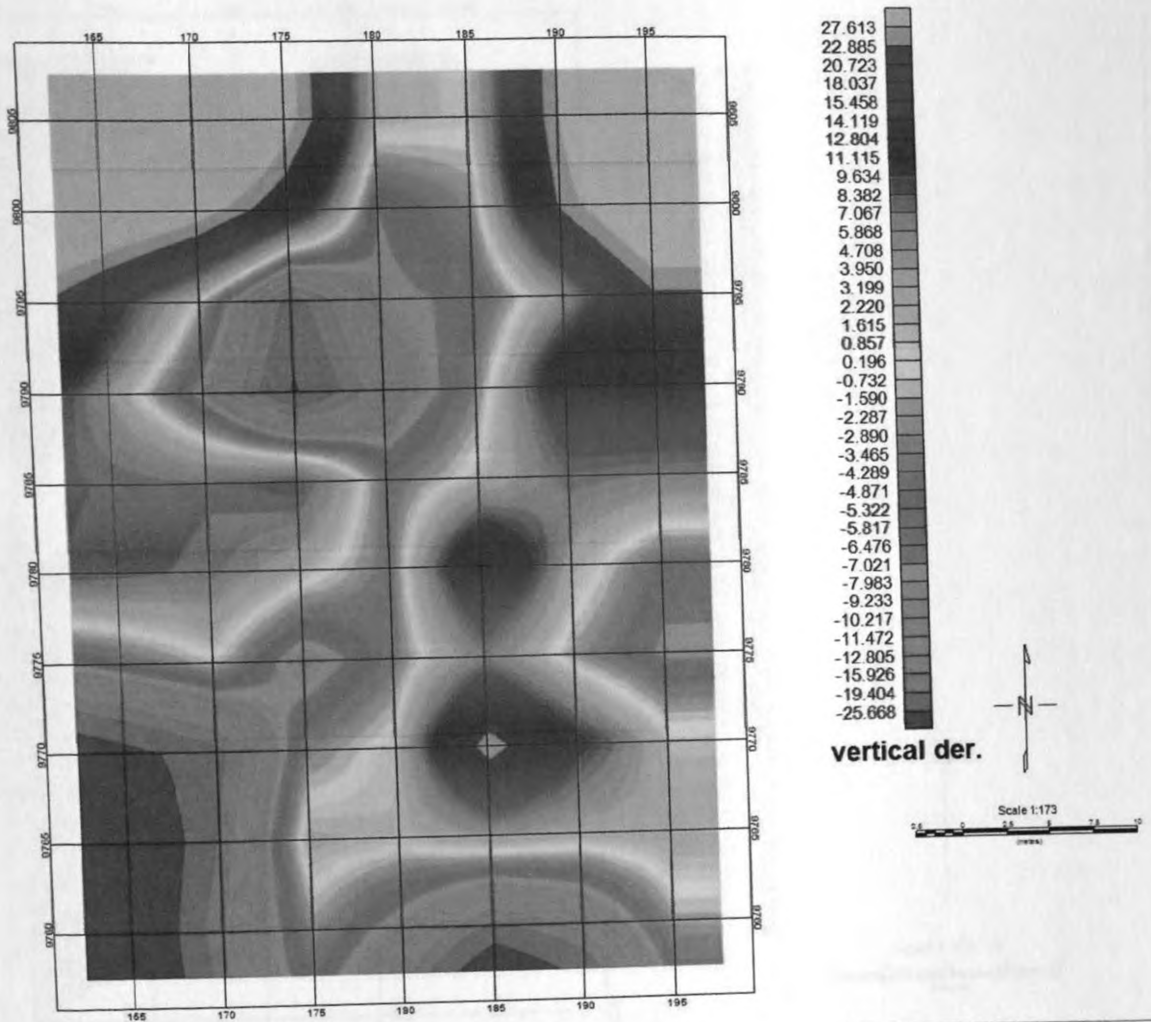


**Figure 5.4: Analytical Signal Map. A grid cell size of 5 was used in obtaining the analytical signal map.**

The analytical signal map gives boundaries of anomalous bodies, within the sedimentary basin, showing that the area is composed of anomalies of varying densities. The anomalies of strong analytical signals are highly concentrated on the north western, north eastern, south western and western parts where gravity values of between 15.187 and 101.971 were observed. These anomalies of weak analytical signals, trend in NE-SW. However, other anomalies are found on the eastern, northern and southern parts of the map, where analytical



Signal values of between -1.174 and 14.89 were recorded. The analytic signal sharpened and enhanced regional structure and their edges.



Geology Department
Vertical derivative map
Magadi Area
Omorho Philip

### Figure 5.5: Vertical Derivative Map

Vertical derivative map can be obtained in different orders. In this study vertical derivative of order one was used to generate the map with a grid cell size of 5. From the map, both deep structures and shallow structures are enhanced, showing that the technique of vertical derivative is to enhance all anomalies with no suppression. Some of the structures which were exposed in upward continuation map are also exhibited in vertical derivative map, in which the deeper structures like the dykes mentioned in figure 5.2 decreased in size and shape with



gh resolution. This supports the argument that vertical derivative enhances shallow anomalies more than the regional anomalies.

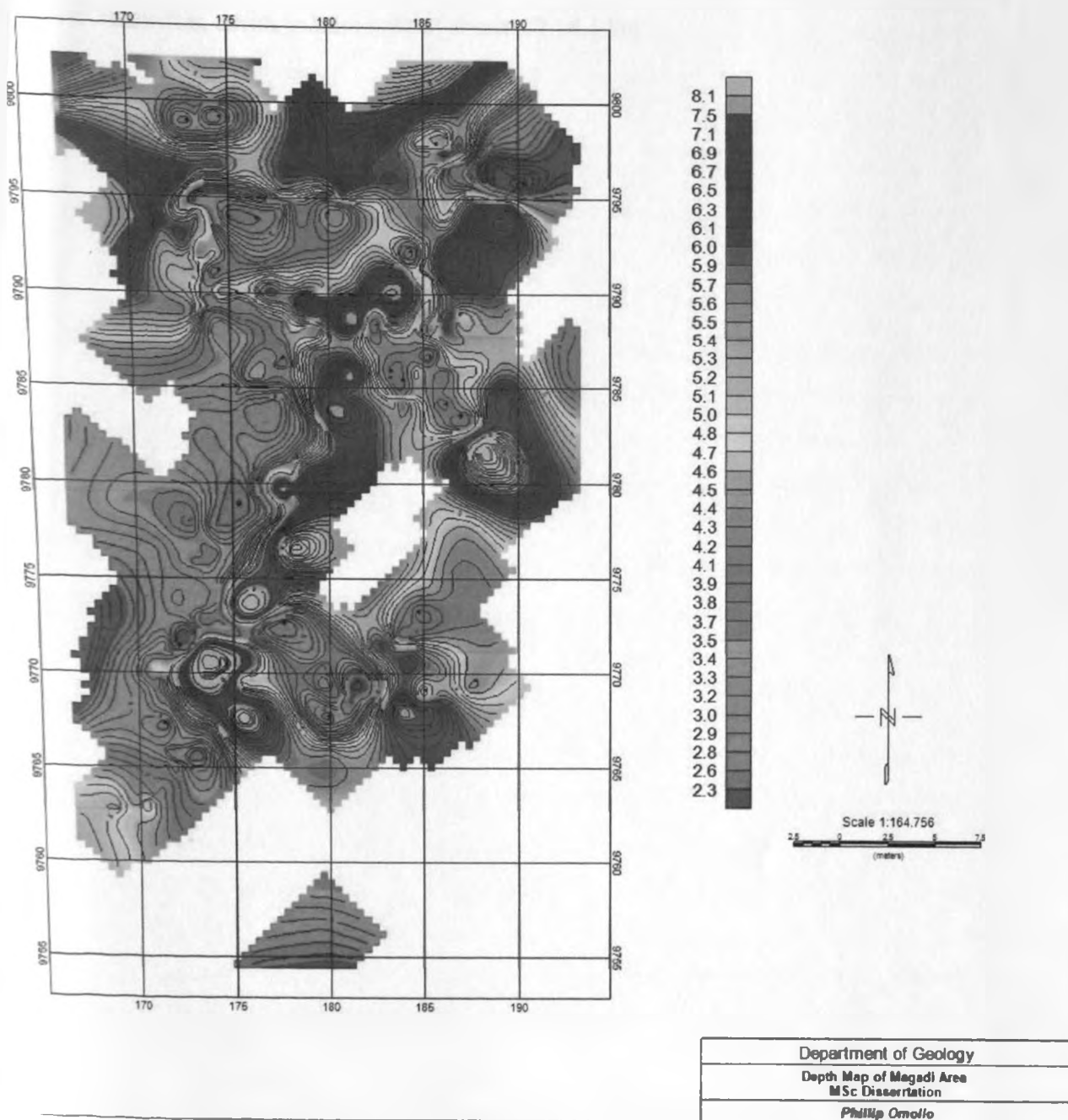


**Figure 5.6: 3D Euler Deconvolution Depth Map at a grid cell size of 5**

The 3D Euler deconvolution map (figure 5.6) shows that the area has a depth to basement ranging from 2 - 8.1 km. The southern part records an average depth to basement ranging

from 2.6 - 5.0 km with some section showing great depth to basement of about 6.5 - 8.1 km. The western section records depth to basement of about 2.3 - 3.5 km. The eastern side indicates depth to basement of about 3.5 - 5 km while some regions indicating depth to basement of 6 - 8.1 km. The central region indicates the deepest section in the area trending in NE-SW recording depth to basement of about 6.7 - 8.1 km.

## CHAPTER SIX

### 6.0. DISCUSSIONS, CONCLUSIONS AND RECOMMENDATIONS

#### 6.1. DISCUSSIONS

The study area is located in tertiary rift sedimentary basin. Sedimentation pertains to accumulation of organic and inorganic sediments. Sedimentary basins are depressions with flat and wide bottoms in which sediments accumulate in ocean or in sea or on land.

The study area has been subjected to sedimentation, volcanism, various erosion activities and various tectonic activities caused by East – West stress. Tectonics in Magadi trough is as a result of discovery of the seismotectonic structures (Behr and Röhricht, 2000). Baker (1958, 1963) and Eugster (1969, 1986) stated that tectonic activity in Magadi region rested after depression of Oloronga beds. Oloronga beds are predominantly found in the southern part of Lake Magadi. According to Behr and Röhricht (2000) deposition of Oloronga bed caused tectonic activities to migrate to the north, which is the reason why tectonic activities are highly recorded in the northern side of Magadi.

Data interpretation was done using Geosoft Inc., Oasis Montaj in which complete Bouguer anomaly map and other interpretation maps were produced.

The Bouguer gravity data were gridded using the minimum curvature technique (Briggs, 1974), then contoured to produce complete Bouguer anomaly map (figure 5.1). A grid cell size of 5 was used in all the maps generated. The study area was clearly delineated as shown in figure 5.1. Most of the anomalies are trending in NE-SW. The central part of the map showed low contours values, mostly trending in NE-SW direction as marked by cold zone (green and blue colours) on the maps. To the Western and Eastern flank of the central part there are closely spaced contours showing a steep gradient. These are suggested to be the edges of the fault.

The fault seems to widen in the Northern part of the study area and narrows as it trends in NE-SW. The widening is marked by gravity low areas labelled F and L on the map, figure 5.1. The study showed that the areas on the southern side are not well defined. The southern part of the Map also indicate the presence of a fault trending in NW- SE forming a junction with the NE-SW trending fault at area labelled L. Between zone F and L exist another gravity

A body labelled B in figure 5.1. This body shows that contours to its western side are closer than those to the eastern side, an indication of steepness to the western side than to the eastern side. In the South eastern part of the area, data coverage was scarce and therefore the structural trend could not be clearly defined.

Both structure F and L attains a gravity low of -1900 mGal while structure B has a gravity low of -1885 mGal. The gravity low values are bounded by gravity high contours trending in the NE-SW direction. The value of gravity is highest to the Eastern and to Western part of study area. These highs could be due to basalt and trachyte of Nguruman escarpment to the west and presence of trachyte on the Eastern side (figure 2.1).

Apart from the main anomalies, there were low and high gravity anomalies which are small in size and could indicate geological structures. They are located about N350°W and S160°E (figure 5.2).

The upward continuation map was generated by a continuation of 1 km, this was done at this distance, because most regional anomalies were highly enhanced compared to continuations done below or above it. In order to delineate a lateral boundary due to main sources of gravity responses, edge enhancement techniques based on gravity signal derivatives; horizontal, vertical derivatives and analytical signals were used. These techniques are commonly used to locate lateral boundaries of density contrasts and provide information on the location of geological units (Blakely and Simpson, 1986).

The amplitude of the enhanced horizontal gradient (Fedi and Florio, 2001) was used to analyse the gravity anomalies which showed its effectiveness in producing higher resolution results, than other edge detection techniques (figure 5.3). This procedure tends to increase signal amplitudes of short wavelength compared to those of long wave length. The horizontal gravity gradients are devoid of topographic influences and locate better than vertical gradients of buried shallow masses. The maximum value of the horizontal gradient tends to be located on the horizontal edge of the gravity source marked with rapid change in density values (Annechhione, 2000; Dhifi et al., 2003; Mohamed et al., 2011).

Since upward continuation enhances regional anomalies, while horizontal derivative defines the boundary at depth of the subsurface anomalies, it was hard to show these anomalies in the complete Bouguer anomaly map before application of upward continuation and horizontal

atives techniques. The horizontal derivatives also showed various bodies to be disjointed basement, with high gravity anomalies closer to the surface than low gravity anomalies to basement. The low gravity anomalies concentrate highly within the faults trending in NE-SW and SE-NW, and appear to represent zones of maximum sediment thickness. The sediments appear to deepen towards the faults (figure 5.1 and 5.2) as can be inferred from the broadening of the anomaly signature and decrease in gradient.

Analytical signal is a method which enhances gravity data and is good since its amplitude function is an absolute value, and no assumption is made in locating the direction of the source body. It is also used to locate edges, reveal anomalies texture, highlight discontinuities (Macleod et al., 1993), and enhances edges of structures as in figure 5.4. Analytical signal technique reduced complete Bouguer anomaly data map to Analytical signal data map, resulting to anomalies whose maxima mark the edges of causative bodies. Analytical signal map aids the horizontal derivative by clearly showing the extent of the anomaly edges or boundaries.

The vertical derivative was used to aid the interpretation process by enhancing and sharpening both regional and local anomalies. The method was found to be effective in locating source bodies (Cooper and Cowan, 2004; Akinola, 2010). The high values of vertical derivative depict shallower anomalous body while vertical derivatives of low value exhibit deeper anomalies. Vertical derivative was lowest in the southern and northern part of the area (figure 5.5), recording values of -25.688 to -1.89, showing these as regions of great depths to basement.

Euler deconvolution is an inversion method for estimating location and source depth. It relates the gravity field and its gradient components to the source of anomaly location with the degree of homogeneity expressed as a structural index, and it is the best method suited for anomalies caused by isolated and multiple sources (El Dawi et al., 2004 and Akinola, 2010). The 3D Euler was done on the gravity field data using standard Euler deconvolution. This was done to locate depth to basement in the study area. The Euler depth was achieved using solution window size of 5, structural index of 1 and 15% depth tolerance (figure 5.6). The window size of 5 km was used because it managed to produce better resolution that best reflects the overall basement structures and accurate estimate of depth to basement. From the Euler depth map, the study area records a maximum depth to basement of about 8.1 km, and a

minimum depth to basement of about 2 km. The deeper area is mainly on the northern and north western sections, while the shallow area is to the western section of the study area.

## 6.2. CONCLUSION

Geophysical methods are important in exploration and geotechnical work. Magadi area being part of tertiary rift system in Kenya, bordering Tanzania to the south, has had a lot of geophysical prospecting which include geothermal investigation, hydrology investigation, and locating Tanzania Craton and Mozambique belt suture. It is evident from the maps of analytical signal, upward continuation and complete Bouguer anomaly that there exists a fault trending in the NE-SW direction associated by depocenters.

The main purpose for this study was to map depocenters. The fault trends in NE-SW showing that the area has been subjected to tectonic activities. This greatest depth to basement in the area of study is about 8.1 km, and the orientation of the hot (red and orange) colours on the map indicates the presence of a fault traversing in the NE-SW direction. A probable dyke was found to exist on south eastern side of the study area in the complete Bouguer anomaly map (labelled D).

Presence of faulting indicates that the study area is experiencing east –west extensional stress. The fault is to a depth of about 8.1 km from the surface. The Northern part and the southern part of the study area shows a region of gravity low and are at a depth of about 8 km to 6 km, these are the depocenters. Interpretation of the maps indicates that there are well developed structures in the basin. The major sedimentary sequences are on the northern and southern parts of the study area stretching to Tanzania.

The presence of depocenters, faults and intrusive bodies are evident showing that the area can have good hydrocarbon occurrence. On the Western and Eastern sides of the study area, the gradient is stronger due to high density contrast between sediment cover and trachyte than on the Northern and Southern parts of the study area.

From the upward continuation, analytical signal, horizontal derivative and vertical derivative maps, it shows that the bodies of low gravity are prevalent in the study area than those of high gravity, an indication that the area is highly covered with the sediment. The fault which results due to tectonic movement accommodates thick sediment with the thickest part

recorded in the northern and southern part of the study area. The deepest section trending in the NE - SW, and traversing the middle part of the Euler 3D map, with recorded depth value of 8.1 km is a fault. The other fault is indicated both in Euler 3D map and Complete Bouguer anomaly map trending NW-SE to the southern part of the study area.

### **6.3. RECOMMENDATION**

From this study, I therefore recommend that more intense work to be carried out in the area. This is to be done by geologist, geochemists and further techniques in geophysical hydrocarbon exploration, like use of seismic methods, to be employed to support gravity data results for thorough delineation of Magadi trough.

## REFERENCES

- Akinola, A.K. 2010. Investigation into the Tectonic Lineaments and Thermal Structure of Lake Magadi, Southern Kenya Rift Using Integrated Geophysical Methods, International institute for Geo-information Science and Earth observation. ENSCHED, The Netherlands, Thesis.
- Annechhione, M.A. 2000. La contribution de la gravimétrie à l'étude hydrogéologique de la Moraine OAK Ridgers. Mémoire de Maîtrise, Université de Montréal.
- Ansari, A.H. and Alandar, K. 2009. Reduction to the pole of magnetic anomalies using analytical signal, world applied journal. 7(4) 405-409 ISSN 1818-1952.
- Ashcroft, W.A., Hurst. A. and Morgan, C.J. 1999. Reconciling gravity and seismic data in the Faero-Shetland basin, West Shetland in: Petroleum geology of Northwest Europe: proceeding of the 5<sup>th</sup> conference (eds A.J. Fleet and S.A.R Boldy), pp 595-600. Geological society of London.
- Atmaoui, N., and Hollnack, D. 2003. Neotectonics and extension direction of southern Kenyan rift, Lake Magadi area: Tectonophysics, V,364, p. 71-83.
- Baker, B.H. 1958. Geology of the Magadi area, degree sheet 51, S.W. Quarter. Geological survey of Kenya, Nairobi. Rep 42: 1- 81.
- Baker, B.H. 1963. Geology of the area south of Magadi. Report Geological survey of Kenya Rep 61:1 52. The Government printer, Nairobi.
- Baker, B.H. 1986. Tectonics and volcanism of the southern Kenya Rift Valley and its influence on rift sedimentation. Geological Society, London, v.25; p45-57.
- Baker, B.H., and Mitchell, J.G.1976. Volcanic stratigraphy and geochronology of the Kedong-Olorgesailie area and the evolution of the south Kenya rift valley. Journal of Geological society, v.132; p467-484.
- Barbosa, V.C.F and Silva, J.B.C. 2011. Reconstruction of geological bodies in depth associated with a sedimentary basin using gravity and magnetic data, Geophysical prospecting journal vol. 59.



Behr, H.J., and Röhrlich, C. 2000. Record of seismotectonic events in siliceous cyanobacterial sediments (Magadi cherts), Lake Magadi, Kenya. Springer – Verlag 2000. *Int J Earth Sci* (2000) 89: 268-283.

Blakely R.J. 1996. *Potential Theory in Gravity and Magnetic Applications*. Cambridge University Press.

Blakely, R.J., and Simpson R.W. 1986. Approximating edges of source bodies from magnetic or gravity anomalies. *Geophysics* 51, 1494–1498.

Bosworth, W., Lambiase, J., and Keisler, R. 1986. A new look at Gregory's rift: structural style of the continental rifting. *EOS*, 576-578.

Briggs, I. 1974. Machine contouring using minimum curvature. *Geophysics* 39, 39–48.

Changyou Zhang, Martin, F. Mushayandebvu, Alan B.Reid, J. Derekfair head and Mark, E.O. 2000. Euler Deconvolution of the Gravity tensor gradient data. *Geophysics* vol 65, p512-520

Cordell, L., 1979. Gravimetric expression of graben faulting in Santa Fe country and the Espanola basin, New Mexico. In: Ingersoll, R.V., (Ed.), *Guidebook to Santa Fe country: New Mexico Geol. Soc. Guidebook. 30th Field Conference*, 59–64.

Cooper, G.R.J., and Cowan, D.R. 2004. Filtering using variable order vertical derivative: computer and *Geosciences*, V.30, P. 455-459.

Crossley, R. 1979. Structure and volcanism in the South Kenya rift in: *Geodynamic evolution of the Afro-Arabian rift system*. Academia Nazionale Dei Lincei, Rome.

Department for international development (DFIH), October 2002. Realising the economic development and poverty alleviation potential of nature in Magadi. Paper.

Dewangan, P., Ramprasad, T., Ramana, M.V., Desa, M., and Shailaja, B. 2007. Automatic interpretation of magnetic data using Euler deconvolution with nonlinear background. *Pure appl. Geophys*, 164; 2359 – 2372.

Dhifi, J., Inoubli, M.H., Ben Jemia, M.G. and Tlig, S. 2003. Gravity contributions to structural modelling of the Sahel platform (Tunisia). 1st North Africa/Mediterranean Petroleum & Geosciences Conference, T006.

Dobrin, M.B., and Savit, C.H. 1988. *Introduction to Geophysical prospecting* 4<sup>th</sup> Edition. McGraw Hill Book Co.

- El Dawi, M.G., Tianyou, L., Hui, S., and Dapeng, L. 2004. Depth estimation of 2-D magnetic anomalous source by using Euler deconvolution method: American Journal of applied sciences.
- England, R.W., McBride J.H. and Hobbs, R.W. 2005. The role of Mesozoic in the opening of the NE Atlantic: Evidence from deep seismic profiling across the Fareo-Shetland trough. *Journal of Geological society* 162, pp 661-673.
- Eugster, H.P. 1969. Inorganic bedded charts from Magadi area, Kenya. *Contrib mineral.*
- Eugster, H.P. 1986. Lake Magadi, Kenya a model for rift valley hydrochemistry and sedimentation geological society, London, special publication v.25 pg 177-189.
- Fairhead, J.D., and Green, C.M.1994. Application of semi-automated interpretation methods in western Siberia and southern Sudan. 56th EAEG meeting, Vienna, Extended abstracts.1037.
- Fedi, M. and Florio, G. 2001. Detection of potential fields source boundaries by enhanced horizontal derivativemethod. *Geophysical Prospecting* 49, 40–58.
- Florio, G., M. Fedi and Pasteka, R. 2006. The application of Euler deconvolution to the analytic signal: *Geophysics* 71, L87–L93.
- Gadalla, M., and Fisher, R. 2009. *Exploration geophysics*, springer-verlag Berlin Heselberg.
- Githinji, J.G., Patel, J.P., Barongo, J.O. and Karanja, P.K. 2011. Application of Euler Deconvolution Techniques in determining depths to Magnetic structures in Magadi area, Southern Kenya Rift. *Jagst* vol.13 (1).
- Gregory, W. 1921. *The rift valleys and geology of East Africa*, pp. 479 Seeley Service London.
- Hassan, S.N., Mohammad, H. H., Mohammed, K., and Farooq A. S. 2009. Stratigraphy, deposition, and structural framework of the cretaceous (Review) and 3D geological model of the lower cretaceous reservoirs, Masila oil field, Yemen. *Arab J geosci* (2010) 3:221-248 Saudi society for geosciences.

Ibs-von Seht, M., Blumenstein, S., Wegner, R., Hollnack, D., and Wohlenberg, J. 2001. Seismicity, seismotectonic and crustal structure of the southern Kenya Rift – new data from Lake Magadi area: *Geophysical journal Int.*, v.146, p. 439 – 453.

Jacobsen, B.H.1987. A case for upward continuation as a standard separation filter for potential-field maps. *Geophysics* 52, 390–398.

Jones, B.F., Eugster, H.P., and the Rettig, S.L.1977. Hydrochemistry of the Lake Magadi Basin, Kenya: *Geochimica et coshimica Acta*, v.41, p. 53 – 72.

Kearey, P., Brooks, M. and Hill, I. 2002. *An Introduction to Geophysical Exploration* third. blackwell science Ltd

Keating, P. and Pilkington, M. 2004. Euler deconvolution of the analytical signal and its application to magnetic interpretation. *Geophysical prospecting* 52, 165-182.

Kuria, Z.N. 2011. *Seismotectonics of active faults: Magadi fault system, Southern Kenya rift* (Dissertation submitted to the University of Twente 29<sup>th</sup> September 2011 ).

Kuria, Z. N., Woldai, T., Meer, F.D. V.D., and Barongo, J.O. 2009. Active fault segments as potential earthquake sources: inferences from integrated geophysical mapping of Magadi fault system, southern Kenya rift: *Journal of Africa Earth Sciences*, v. in press, corrected Proof.

Lambiase, J. J., and Bosworth, W. 1995. Structural controls and sedimentation in continental rift. *Geological society, London, special publication* v. 80.

Le Gall, B., Tiercelin, J.J., Richert, J.P., Gente, P., Sturchio, N. C., Stead, D., and Le Turdu, C.2008. A morphotectonic study of an extensional fault zone in a magma rich rift: Baringo trachyte fault system, central Kenya rift. *Tectonophysics*, 320, 87-106.

Le Turdu, C., Tiercelin, J.J., Richert, J.P., Rolet, J., Xavier, J.P., Ranaut, R.W., Lezzar, K.E., and Coussement, C. 1999. Influence of pre-existing oblique discontinuities on the geometry and evolution of extensional fault patterns; evidence in the Kenya rift using spot imagery in: C.K. Morley (editor), *Geoscience of rift system. Evolution of east Africa: AAPG study in geology*, P. 173-191.

Lerner, E.K.L., and Cengage, B.W.L.G. 2003. *Faults and Fractures*, World of earth science.

- Levorsen, A.I. 1985. *Geology of petroleum*, CBS Publishers and Distributors 4596/1-A, 11 Darya Ganj, New Dehli-110002 (India).
- Macleod, I.N., Jones, K., and Dai, T.F. 1993. 3D analytical signal in the interpretation of total magnetic field data at low magnetic latitudes: *Exploration Geophysics*, V. 24, P. 679-688.
- Maguire, P.K.H., and Long, R.E. 1976. The Structure of Western flank of Gregory rift (Kenya). Part I. The crust: *Geophysical Journal of the Royal Astronomical society*, v.44, p.661-675.
- Majid, B. 2010. The analytical signal of gravity tensor and their application to estimate source location. *Geophysics*, vol. 75. 159-174.
- Marita, N.O. 2007. *The gravity and magnetic methods UNU-GTP-KenGen Geothermal training manual*.
- Marson, I., and Klingel, E.E. 1993. Advantages of using the vertical gradient of gravity for 3-D interpretation. *Geophysics* 58, 1588-1595.
- Mohamed, A., Mohamed, H., Sa'id, T., and Rabeh, A. 2011. Gravity analysis of salt structures. An example from the El Kef-Ouargha region (northern Tunisia). *Geophysical Prospecting*, 2011, 59, 576-591.
- Molnar, p., and Aggarwal, Y.P. 1971. A micro earthquake survey in Kenya: *Bulletin of the Seismological society of America*, v. 61, p. 195 - 201.
- Nabighian, M. N., Grauch, V.J.S., Hansen, R.O., La Fehr, T.R., Li, Y., Peirce, J.W. 2005. The historical development of magnetic method in exploration, *Journal Geophysics*, 70, 33ND-61ND.
- Omenda, P.A. 2007. *Status of Geothermal Exploration in Kenya and Future Plans for its development*, KenGen, Naivasha, Kenya.
- Petar, Y.S. 1997. Euler deconvolution using differential similarity transformation using differential similarity transformation of gravity or magnetic anomalies. *Geophysical prospecting* 45, 207-246.

- Peterson, N.R., and Reeves, C.V. 1985. Application of gravity and magnetic surveys. The state of the art in 1985, *Geophysics* 50, 2558-2598.
- Reid, A.B., Alsop J.M., Grander H., Millet, A.J., and Somerton, I.W. 1990. Magnetic interpretation in three dimensions using Euler deconvolution. *Geophysics* 55, 80–91.
- Roest, W.R., Verhoef, S.J., and Pilkington, M. 1992. Magnetic interpretation using the 3D Analytical signal. *Geophysics*, 57, 116-125 (Edited by Kuria, 2010).
- Sequar, G.W. 2009. Neotectonics of the east African rift system: new interpretation from conjunctive analysis of field and remotely sensed datasets in the lake Magadi area, Kenya, Enscheda, ITC.
- Silas, M.S. 1996. Intergrated geophysical study of the crustal structure of the southern Kenya Rift, pp. 68-72.
- Simiyu, S.M and Keller, R.G. 1998. Upper crustal structure in the vicinity of Lake Magadi in the Kenya rift valley region. *Journal of African earth sciences*, 27, 359-371.
- Smith, M., and Mosley, P. 1993. Crustal heterogeneity and basement influence on the development of the Kenya rift, East Africa. *Tectonics*, 12, 591-606.
- Stavrev, P., And Reid, A. 2007. Degree of homogeneity of potential fields and structural indices of Euler deconvolution. *Geophysics* 72, L1 – L12.
- Steenland, N.C. 1968. Discussion on "The geomagnetic gradiometer "by H.A. Slack, V.M. Lynch and L. Langan (*Geophysics* 32, 877–892). *Geophysics* 33, 681–684. (edited by El sayed).
- Tatiana, A. M. Q. 2009. Euler homogeneity equation along ridges for a rapid estimation of potential field source properties. *Geophysical prospecting journal* V59, 527-542.
- Telford, W., Geldart, L.P., and Sheriff, R.E. 1990. *Applied Geophysics*, Cambridge university press.
- Thompsons, D.T. 1982. EULDPH: A new technique for making computer assisted depth estimates from magnetic data. *Geophysics* 47, 31-37.

Wolfgang, J.J and Peter, L.S. 2009. Fundamentals and application inversion and geological interpretation.

Zhaofang, Z. 1994. Interpretation of aeromagnetics data using 3D Euler deconvolution and 3D analytical signal in the Qinling orogenic belt, China. 56th EAEG meeting, Vienna, Extended abstracts, p005.



**B. Gravity Data of Magadi Basin Covering the Study Area (NOCK, 1974)**

station No	grid East	Ref. (KM.) North	long degrees	lat degrees	Height value	(H.) ACC	Observ gravity	TER .CO R	F.A.A	S.B.A	C.B.A
4800	175.	9796.	36.087	-1.8362	662.9	1	977718	26	-1144	-1886	-1867
4801	173.	9798.	36.069	-1.8217	683.7	1	977717	43	-1083	-1848	-1812
4802	172.	9799.	36.059	-1.8135	737	1	977708	52	-1008	-1833	-1789
4803	171.	9800.	36.046	-1.8063	791.9	1	977700	77	-923	-1809	-1740
4804	170.	9800.	36.041	-1.8063	796.1	1	977701	112	-901	-1792	-1688
4799	177.	9795.	36.101	-1.8471	650.4	1	977719	19	-1167	-1895	-1883
7033	191.	9798.	36.23	-1.8238	625.5	2	977737	6	-1069	-1769	-1770
7034	190.	9800.	36.220	-1.803	658.3	2	977729	5	-1040	-1777	-1779
7037	186.	9796.	36.186	-1.8418	721.7	2	977714	5	-1004	-1812	-1815
7038	184.	9795.	36.166	-1.8463	665.7	2	977722	7	-1090	-1835	-1835
7039	183.	9794.	36.153	-1.8562	645.6	2	977724	9	-1133	-1855	-1853
7040	190.	9795	36.131	-1.8525	661	2	977720	11	-1131	-1871	-1867
7041	177.	9795.	36.101	-1.8471	653	2	977719	19	-1161	-1891	-1879
7042	175.	9797	36.084	-1.8344	661.8	2	977718	28	-1147	-1888	-1867
7043	173.	9798.	36.068	-1.8199	712.1	2	977713	41	-1041	-1838	-1805
7044	171.	9800.	36.045	-1.8063	791.3	2	977701	86	-911	-1796	-1719
7045	175.	9792.	36.083	-1.8723	654.9	1	977716	25	-1191	-1924	-1906
7046	175.	9789.	36.082	-1.8985	649.4	2	977718	22	-1191	-1918	-1903
7047	175.	9786	36.085	-1.9338	640.9	2	977728	17	-1118	-1835	-1825
7048	174.	9783.	36.070	-1.95	631.5	2	977735	19	-1073	-1780	-1768
7049	171.	9779.	36.050	-1.9943	621.7	2	977734	23	-1121	-1817	-1801
7057	178.	9799.	36.108	-1.8109	673.3	2	977714	18	-1144	-1898	-1887
7036	190.	9794.	36.214	-1.8572	710	2	977717	5	-1005	-1799	-1802
7060	181.	9790.	36.137	-1.8941	642.3	2	977723	9	-1156	-1875	-1873
7061	183	9786.	36.150	-1.9312	632.3	2	977728	7	-1144	-1851	-1852
7062	183.	9782.	36.157	-1.9655	626.4	2	977734	6	-1100	-1801	-1803
7063	184.	9779.	36.166	-1.9927	620.6	2	977738	5	-1083	-1777	-1779
7560	178.	9792.	36.112	-1.8787	647.7	2	977719	14	-1183	-1908	-1901
7561	189.	9791.	36.207	-1.8834	682.7	2	977725	4	-1014	-1778	-1781



7562	187.4	9787.9	36.1904	-1.9168	667	2	9777303	4	-1014	-1761	-1764
7563	188	9784.8	36.1957	-1.9448	676.6	2	9777290	3	-1000	-1757	-1761
7564	189.5	9781.8	36.2091	-1.9719	660.8	2	9777335	3	-1005	-1745	-1749
7565	191.7	9779.5	36.2289	-1.9928	602.6	2	9777462	4	-1060	-1734	-1737
7566	192.1	9784.4	36.2325	-1.9485	651.5	2	9777368	4	-1000	-1729	-1733
7556	179.8	9780.8	36.122	-1.9808	620.6	2	9777320	8	-1145	-1840	-1839
7557	175.7	9780.8	36.0852	-1.9808	619.5	2	9777330	13	-1139	-1832	-1826
7558	178.3	9783.3	36.1086	-1.9582	625.7	2	9777296	10	-1152	-1852	-1849
7559	180.1	9786.9	36.1248	-1.9257	628.3	2	9777271	10	-1167	-1870	-1867
7532	184	9797.8	36.16	-1.8273	657.1	2	9777235	9	-1109	-1844	-1842
7050	170.3	9775.7	36.0366	-2.0268	619.6	2	9777375	18	-1096	-1789	-1778
7064	185.8	9775.3	36.1758	-2.0306	617.8	2	9777414	3	-1063	-1754	-1758
7065	189	9774	36.2045	-2.0424	634.5	2	9777413	3	-1013	-1723	-1727
7066	191.5	9775.3	36.2279	-2.0307	626.2	2	9777427	3	-1024	-1724	-1728
7534	169.9	9773.2	36.033	-2.0493	623.5	2	9777386	13	-1074	-1772	-1765
7535	170.1	9770.4	36.0347	-2.0746	600.8	2	9777341	10	-1191	-1864	-1860
7536	171.2	9767.2	36.0445	-2.1036	598.6	2	9777315	9	-1225	-1895	-1893
7537	171.8	9764.6	36.0499	-2.1271	599.4	2	9777346	12	-1193	-1864	-1859
7538	174.3	9766	36.0724	-2.1145	629.6	2	9777311	32	-1135	-1839	-1815
7539	176.3	9768.7	36.0904	-2.0901	605.3	2	9777376	13	-1143	-1820	-1814
7540	179.8	9769.2	36.1218	-2.0857	608.8	2	9777359	8	-1149	-1830	-1829
7541	182.4	9768.6	36.1452	-2.0911	609.1	2	9777437	5	-1071	-1752	-1754
7542	182.6	9765.2	36.1469	-2.1218	645.3	2	9777324	8	-1074	-1796	-1795
7543	182.6	9761.3	36.1468	-2.1571	705.1	2	9777198	4	-1018	-1807	-1811
7544	186.7	9771.6	36.1838	-2.0641	629.9	2	9777423	3	-1019	-1724	-1728
7545	185.8	9769.6	36.1757	-2.0821	627.7	2	9777433	3	-1016	-1719	-1722
7546	179.9	9771.1	36.1227	-2.0685	608.1	2	9777413	6	-1096	-1776	-1777
7547	181	9773.9	36.1327	-2.0432	612.1	2	9777387	5	-1108	-1793	-1795
7548	178.1	9773.9	36.1066	-2.0432	609.6	2	9777381	7	-1122	-1804	-1805
7549	176.1	9772.2	36.0886	-2.0585	608.4	2	9777374	8	-1134	-1815	-1814
7550	173.5	9769.4	36.0652	-2.0837	603.3	2	9777366	9	-1159	-1834	-1833
7551	173.2	9772.2	36.0626	-2.0584	606.1	2	9777356	9	-1159	-1837	-1835
7552	173.1	9773.4	36.0617	-2.0476	608.1	2	9777342	10	-1165	-1846	-1843
7553	174.7	9777	36.0761	-2.0151	613.7	2	9777311	11	-1178	-1864	-1861
7554	176.4	9776.4	36.0914	-2.0205	612.9	2	9777329	9	-1162	-1848	-1846
7555	179.3	9776.5	36.1174	-2.0197	610.9	2	9777365	7	-1132	-1816	-1816
7568	190	9777.7	36.2136	-2.009	655.6	2	9777358	2	-1001	-1735	-1739